Title
Single-viewpoint, catadioptric cone mirror omnidirectional imaging theory and analysis

Journal
Journal of the Optical Society of America A-Optics Image Science and Vision, 23(12)

ISSN
1084-7529

Authors
Lin, S S
Bajcsy, R

Publication Date
2006-12-01

Peer reviewed

Single View Point Catadioptric Cone Mirror Omnidirectional Imaging Theory and Analysis

Shih-Schön Lin

Electrical and Systems Engineering Department, University of Pennsylvania,

220 South 33rd Street Moore 203 Philadelphia, PA 19104-6390, USA

Ruzena Bajcsy

Center for Information Technology Research in the Interest of Society (CITRIS)

665 Soda Hall, University of California, Berkeley, CA 94720-1776, USA

A family of catadioptric imaging systems has been developed that can achieve omnidirectional view with one single planar imager while still being able to recover perspective pictures, provided that they satisfy the single view point (SVP) constraint. It has been shown that the only mirror shapes that can have SVP when paired with only one single focusing planar imager camera are the surfaces of revolution of conic section curves. However, its special case, the cone shaped mirror itself, has not been deemed as a viable SVP mirror shape. We present the comprehensive imaging theory about the cone mirror in its SVP configuration. We show that the SVP cone mirror catadioptric system not only is practical but also has unique advantages for certain applications. The detailed theory explains why and how a practical SVP cone configuration can be set up, the merits and weaknesses of such systems, and how one can remedy the weaknesses to create a workable imaging system. We also derive the tolerance formula for estimating effects of alignment errors. A prototype is constructed and experimental results validate our theory.

OCIS codes: 110.0110 Imaging systems, 220.0220 Optical design and fabrication, 150.0150 Machine vision, 100.0100 Image processing.

Introduction

Ordinary cameras used in machine vision either have a narrow field of view (FOV) or have a wide FOV but suffer from complex distortion. It can be difficult to unwarp a wide FOV image to perspective projection views accurately. Based purely on the ideal projection imaging model, it has been shown that surfaces of revolution of conic section curves are the only mirror shapes that can be paired with a single converging projection camera to create SVP catadioptric omnidirectional view systems whose omni-view image can be unwarped to perspective projection views without systematic distortions[1]. The pin-hole model based geometry has also been analyzed by others[2-6]. The critical condition to being able to unwarp to perspective projection views from a single omni-view image is to satisfy the single-view-point (SVP) condition[1]. The cone shape, although a surface of revolution of a conic section, was deemed unusable because it seemed that in its SVP configuration "only rays grazing the mirror surface can be seen"[1]. In fact, practical SVP cone mirror omni-view system can indeed be constructed[4,6]; this work is an expansion on the important discovery. We show in this work that even under the pin-hole camera model the SVP cone configuration works and sees any world point in its FOV, not just "rays grazing the mirror surface".

The cone mirror has not been used to construct an SVP omnidirectional imaging sensor that can reproduce perspective projection views from a single omni-view image before our work. However, cone mirrors have been used to aid navigation, map building, collision avoidance, and

pipe inspections in non-SVP configurations[7-11]. The cone mirror images were used 'as is', and no attempt was made to unwarp them to undistorted images. Using multiple normal cameras positioned properly in relation to a plane mirror pyramid, a high resolution SVP wide FOV system can be built[12,13]. The trade offs, though, are the high price and complexities involved with multiple cameras. Bulky size, weight, calibration, synchronization, and gain differences are problems associated with multi-camera systems that single camera systems are free of.

SVP is worthwhile to have if the benefits outweigh the drawbacks for a particular application. Only with SVP can a catadioptric omni-cam use a single range-independent look up table or formula for correct unwarping. The SVP cone system is cheap and simple to build, operate, and maintain while retaining a decent vertical resolution and good flexibility in SVP. The SVP cone system is therefore always worth evaluating before considering more complex and expensive omni-view sensors. The main purpose of our work here is to prove that an SVP cone system is both theoretically and physically viable and to present a detailed analysis for cone SVP systems that provides systematic physics-based guidelines for deciding whether the SVP cone is suitable for a particular application. For applications in which SVP is not critical, Swaminathan, *et al.* have shown ways to recover believable perspective views from non-SVP systems[14]. Rees[15], Bogner[8], Hicks *et al.*[16,17], and Chahl *et al.*[10] have shown several types of non-SVP omnidirectional mirror shapes with interesting properties.

The advantages of the single camera SVP catadioptric family of omnidirectional imaging systems come with a price. The most significant trade-off is a much lower image spatial resolution compared to normal cameras, multi-camera omni-view systems[13], or rotating normal camera scanning systems[18] due to the fact that single camera SVP catadioptric systems have an enlarged FOV without a corresponding increase in the number of physical sensing units (e.g.

pixels). Because of this, Nagahara *et al.*[19] proposed stitching many omni-view images to form a single picture with better resolution. However scanning and stitching cannot be done in real time, though the extra views may be used for omni-stereo[20-24]. Southwell *et al.*[25] used concentric mirrors to get two views in one picture that sacrifices resolution further in exchange for fast omni-stereo. Multiple omni-views may also be captured simultaneously for omni-stereo with the help of beam splitters[26]. Furthermore, when designing a real optical system that conforms to the SVP condition, it turns out that certain optical aberrations tend to be more visible. However, the analysis of this problem cannot be performed under the pin-hole camera model from which the SVP theory was originally derived. Baker and Nayar[1] analyzed some "defocus blur" problems for hyperbolic and parabolic mirrors using a paraxial (Gaussian) optics model plus a fixed position finite aperture. Yamazawa *et al*.[2] and Yagi *et al*.[7] briefly mentioned some more optical problems for convex mirrors including spherical aberration and astigmatism. Ishiguro[27] gave a qualitative summary of aberrations of various single camera SVP catadioptric systems but not for cone mirrors in the SVP configuration.

We analyze here the aberrations of SVP cone mirror systems using accurate numerical optical ray tracing. Based on our analysis we show an optical design that minimizes such aberrations. The cone is among the simplest mirror shapes to produce, and it has much higher meridional (tangential) angular resolution compared with other conic section mirrors for scenes around the horizon[11,27]. It adds the least optical distortion to the resulting meridional images because it is the only omni-view mirror with a non-curved mirror surface in the meridional cross sections.

SINGLE-VIEW-POINT CONE MIRROR IMAGING THEORY

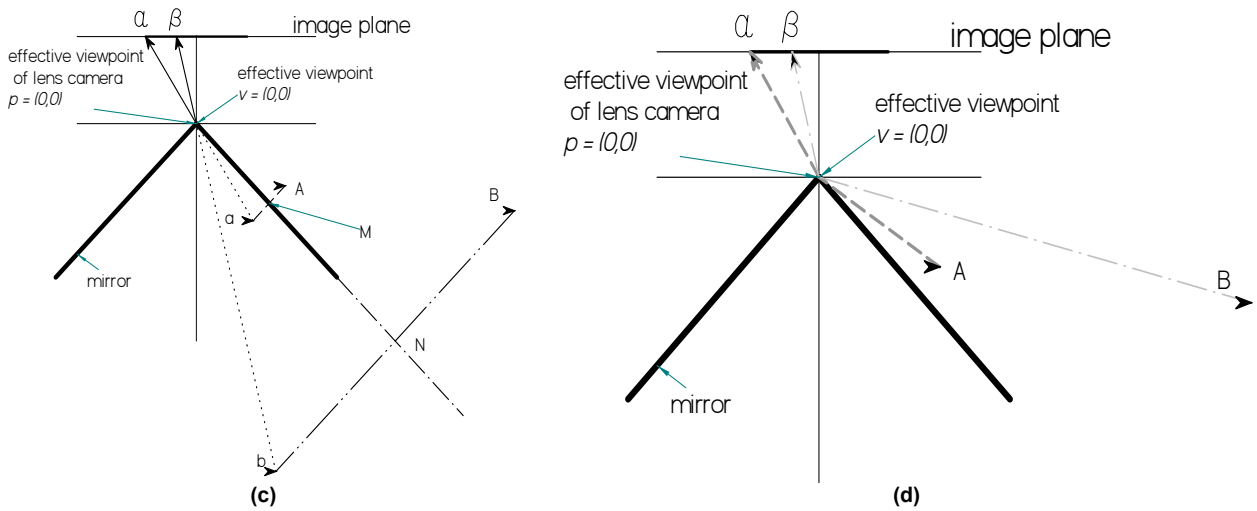

Fig. 1 SVP Cone Mirror imaging model in the pin-hole camera model (a) explained by the concept of "virtual image" (b) explained by direct "ray-tracing".

The concept of "Single-view-point" (SVP) is well defined in the projective pin-hole camera imaging model, where each lens camera is modeled as a point in space (the "projection center" for the lens camera) and an image plane. By definition, all normal lens cameras in the perspective pin-hole model meet the SVP condition. However the SVP concept becomes increasingly less well defined in the context of more physically accurate optical imaging models. In other words, a real lens camera by itself is not SVP in the strictest mathematical sense. They are numerically good approximations of an ideal pin-hole SVP camera only within their published working distances under intended usage. We have to redefine "SVP" in Gaussian optics and study "defocus" caused by "skew rays" using geometric optics[28,29]. We have shown experimentally that SVP cone configuration can indeed capture complete omnidirectional view images[4,6]. Now we show why SVP cone works in the purely theoretical pin-hole model. Then we show progressively how we can extend this concept in more complex optical models.

SVP Catadioptric Cone Omni-cam under the Perspective Pin-hole Model

Fig. 1 illustrates the imaging model of an SVP cone mirror omnidirectional vision sensor system. The imaging process can be described in a few different ways, all of them equivalent but each

sheds light on the related different physical properties. The first description (Fig. 1 a) is based on the concept of a "virtual image." A "Virtual image" of a world point is a point that, when viewed from the position of an observer, seems to be the source point from which all the light of the world point comes. The cross section of cone mirror in any meridional plane as depicted in Fig. 1 a is exactly the same as that of two plane mirrors. Plane mirrors have been proven to be the only mirror shape that produces a perfect virtual image[28,30]. As shown by Baker and Nayar[1], the SVP condition of a cone mirror corresponds to the condition when the viewpoint of a perspective camera coincides with the tip of the cone. The system in Fig. 1 is arranged to have the SVP of the lens camera placed at the SVP of the cone, which is located right at the tip of the cone.

The second way to describe the imaging of the SVP cone mirror system is sometimes called "ray-tracing" (note: "ray-tracing" has a different meaning in the geometric optics model). If we have an algorithm such that given any world point one can trace the light ray via a unique path to a unique image point on the image plane, we have a projection. If every such unique ray path for every given world point passes through the SVP of both the mirror and the camera, we have met the SVP condition. All these ray paths must not violate the law of reflection; however the law of refraction is a non-issue because the lens component is represented by an ideal pin-hole. This is the way the original SVP theory was derived[1]. The cone can also be proven to be SVP by "ray tracing" as shown in Fig. 1 b. Consider any arbitrary world point in Fig. 1 b (point source) in front of the mirror (e.g. point A or B), there always exists a ray that is emitted toward the point at the tip of the cone (point p). Since point p is part of the mirror this ray will be reflected at the point p per law of reflection (and reach point α or point β). The presence of a pin hole is *never* in the way of this process let alone blocking anything. The pin hole placed at point p is in no way to block the ray Ap or Bp. Since the pin hole is a hole that let light pass the

pinhole is not blocking the ray pα or pβ, either. It is clear that any world point inside the normal FOV of the SVP cone system can be imaged without problem, not just "rays grazing the surface of the mirror". The key point is that the tip of the cone serves simultaneously as both the point of reflection on the mirror and as the SVP simultaneously for all scene points. Also note that the points A, B, p, α and β in Fig. 1 a and Fig. 1 b can be placed at exactly the same relative geometric locations. The two descriptions illustrated by Fig. 1 a and Fig. 1 b are equivalent. For more details see[4,6].

The theory of the working SVP cone catadioptric sensor is as follows: the configuration in Fig. 1 has previously been proven to be SVP. The only argument against its practicality is that no image of any world point can be formed on the camera image plane except those along the mirror surface line[1] and we have just addressed this concern by establishing the correct theory of how and why arbitrary world points can be imaged under the SVP condition of the cone mirror. Thus we have derived the theory of an SVP cone mirror catadioptric omnidirectional sensor system under the pin-hole camera model proving that it should work.

SVP Catadioptric Cone Omni-Cam under the Gaussian Optics Model

Gaussian optics, also called first order optics, can be summarized in a concise formula, the Gaussian formula: (s_o: object distance; s_i: image plane distance; f: effective focal length)[28,29]

$$(1/s_o)+(1/s_i)=(1/f) \tag{1}$$

The most prominent change in the lens model is that now we can find more than one "effective viewpoint" or "projection center" for a lens or lens system when we try to fit the perspective projection concepts into the Gaussian optics framework. This is why in Fig. 3 we see two different configurations that are both SVP (see[4,6]).

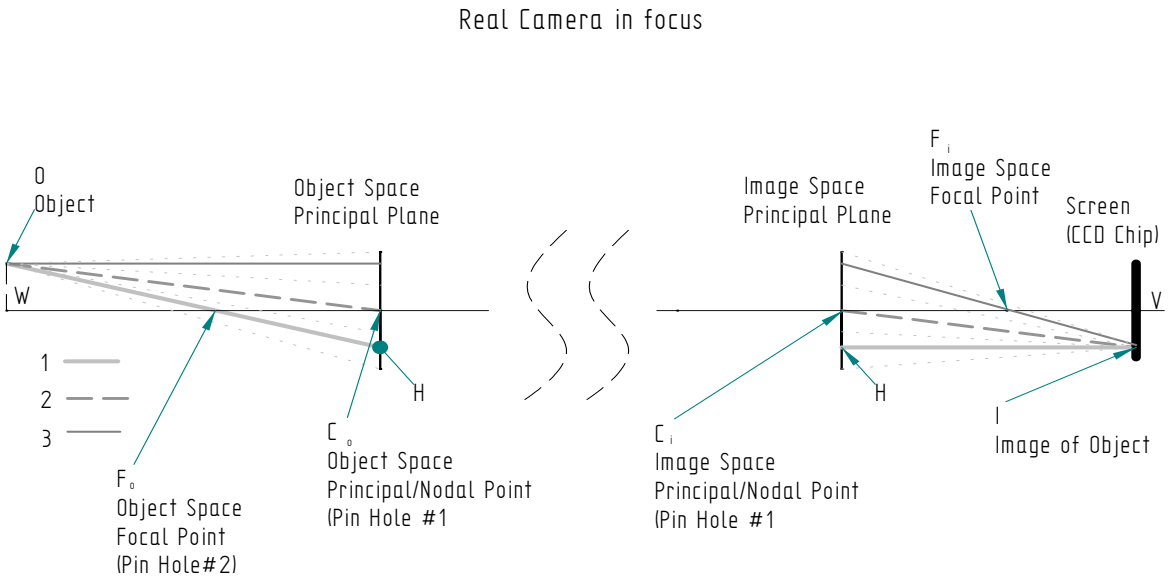

Fig. 2 Multiple "SVPs": Projection centers and principal points of a focusing camera system in Gaussian optics model.

In Fig. 2 we show a more generalized lens/lens set having a world point O in focus with an image formed at the point I. The cardinal points of this optical system are F_o (object space focal point), C_o (object space principal and nodal point), C_i (image space principal and nodal point), and F_i (image space focal point). The Gaussian optics model is more realistic than the pin-hole model in that all the rays originating from a world point are considered. The Gaussian optics model is still a simplification from the real world in that it assumes the optical system can perfectly focus all light rays from the same world point and are collected by the optical system to the same image point. Several special properties for rays passing through cardinal points of the system come from such ideal assumption. First, all rays passing through the object space focal point F_o will appear to continue unaltered to the object space principal plane at point H, and then from the same height measured from the optical axis, it will appear to reemerge at the conjugate image space principal plane and continue parallel to the optical axis until it reaches the image plane at the image point I. For all world points at the same object plane (i.e. the plane that is perpendicular to the optical axis and intersects the optical axis at the point W), their images,

although actually formed on the screen at V, can be orthographically projected to the object space principal plane along the optical axis. Also from every image point one can draw a straight line from the shifted image point passing the object space focal point F_o and reach the corresponding world point. This is exactly the definition for perspective projection with F_o as the projection center. Although strictly true for only world points in one plane, we can as a practical matter relax the Gaussian optics model a little and treat F_o as the projection center for all world points "inside the depth of field." The concept of depth of field and depth of focus arises because all real imaging devices have finite resolution. The smallest CCD sensing unit is a pixel, so a blurring pattern smaller than a pixel cannot be detected. Similarly, traditional films cannot detect blurring smaller than their light sensing particles/compounds.

In fact, there exists a distance, called the hyperfocal distance, such that all world points farther away from the camera than it can be considered in focus. The hyperfocal distance can be calculated by the following formula: (definitions and figures see[28,29])

$$S_{o\_hyperfocal} = f^2/(Ad) = fD/d \tag{2}$$

This formula is derived from several loose assumptions and must be used with caution. However, for our purposes we can say that we have a practical projection center for a lens camera under a slightly relaxed version of the Gaussian optics imaging model.

We can find another practical projection center using the same framework. In Fig. 2 we can use another Gaussian optics rule for the cardinal point C_o, the object side principle point. Namely, any ray that appears to pass through C_o in the object space will appear to emerge from the image side principal point C_i and follows the same propagation direction until it intersects the image plane at I. If we put the two principle planes together, as shown in most illustrations for a single thin lens, we have a perspective projection under the same reasoning as that for F_o.

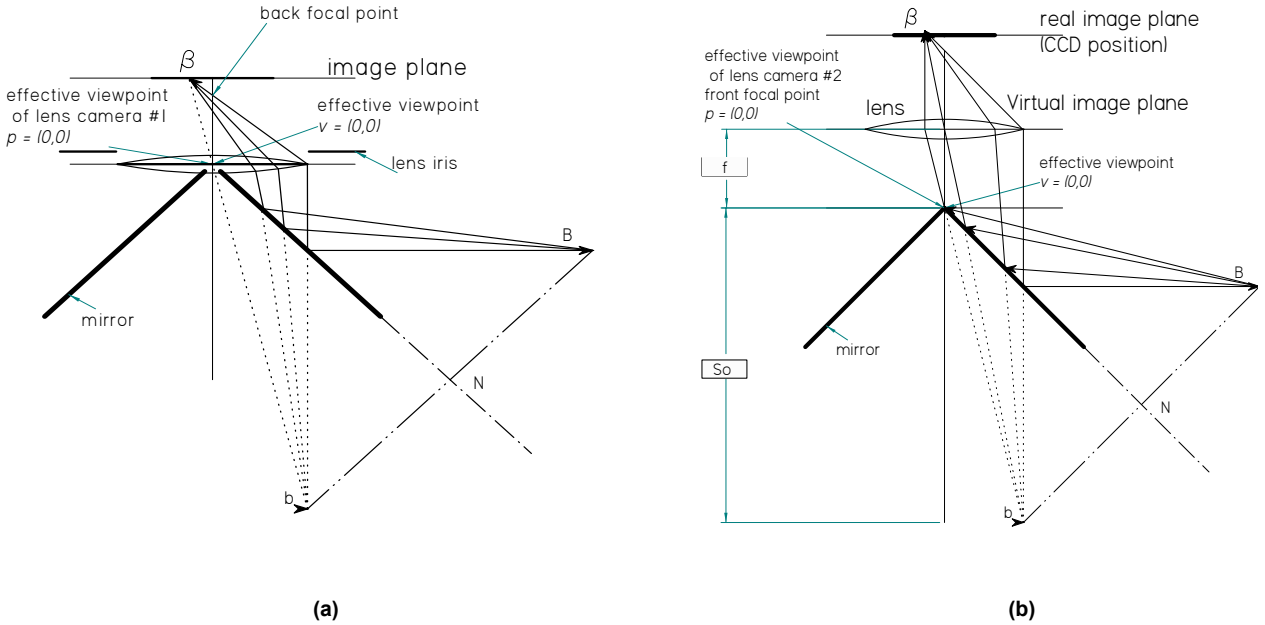

Fig. 3 Meridional ray tracing illustration of two cone SVP configurations. (a) SVP at the cone tip. (b) SVP at front focal point.

In addition, another cardinal point pair, called nodal points, can also be regarded as the effective SVP. In simpler optical systems the nodal points coincide with the principal planes. However this is not always the case. The definition of nodal points is that light passing through the object side nodal point will always emerge from the image side conjugate nodal point(s) with the same light path angle relative to the optical axis. The two conjugate nodal points serve the same functions as the two focal points in hyperbolic and ellipsoidal mirrors in preserving SVP. The main difference is that the nodal point properties hold only in the paraxial region, a condition considered met when the optical system is operating inside the depth of field/focus.

We have thus completed the SVP theory for a lens camera under a imaging model of slightly relaxed Gaussian optics. Using our theory, optical engineers will know where exactly to place the cardinal points in order to preserve the SVP condition.

SYSTEM CHARACTERISTICS

Field of View (FOV)

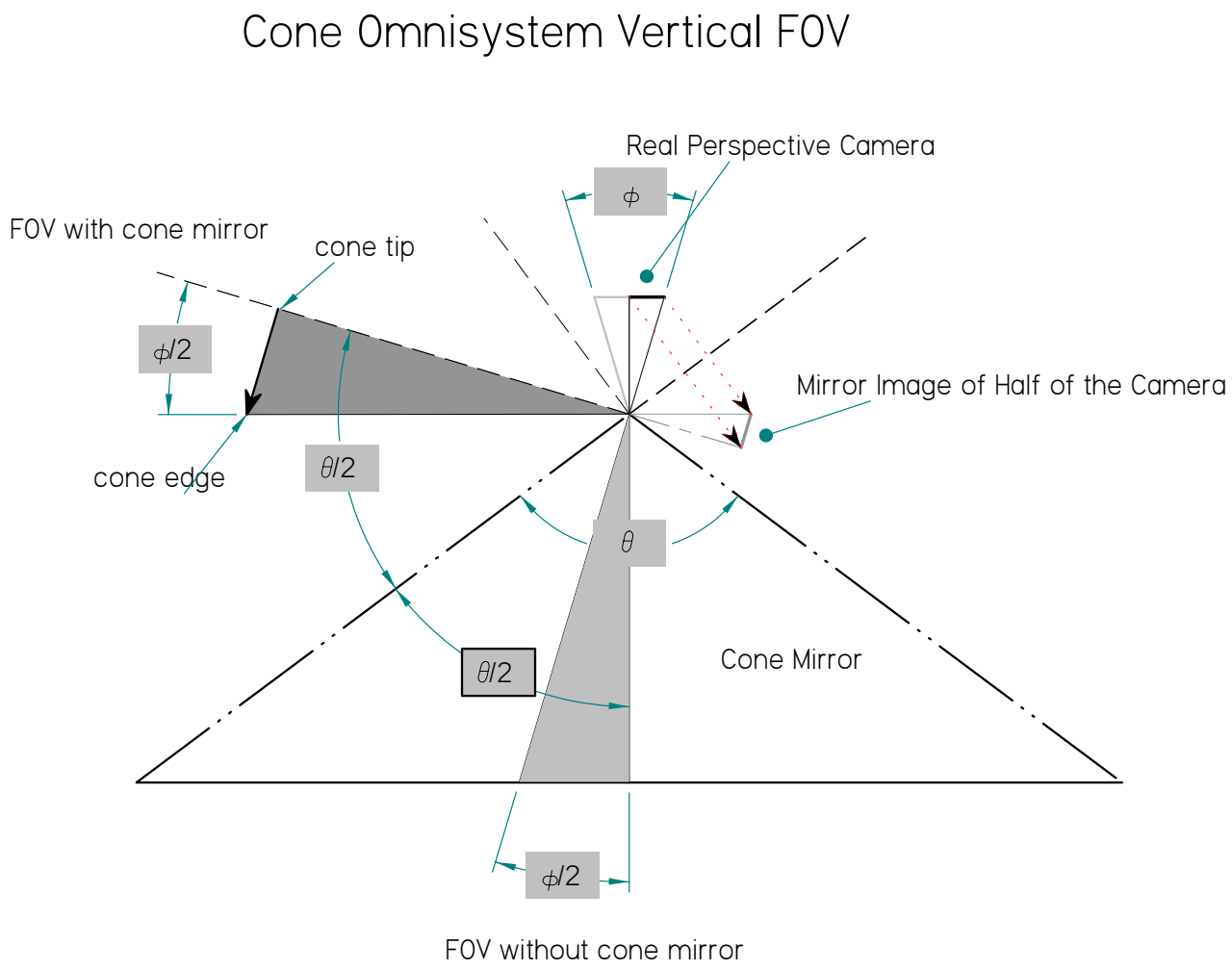

Fig. 4 SVP Cone angular FOV limits determined by the shape of the mirror and the FOV of lens camera

Unlike most existing omnidirectional camera systems, the vertical FOV for cone mirror based omnidirectional camera is not continuous across the zenith. As shown in Fig. 4, if the tip of the cone subtends an angle θ, and the normal angular FOV of the perspective camera is φ, then the upper limit of viewable elevation is $\theta - \pi/2$. The elevation here is defined to be 0 at the horizon, 90 degree straight up and -90 degree straight down, the same system as used for a gun turret. The lower bound of viewable elevation is $\theta - (\pi/2) - (\varphi/2)$. The extent of the vertical FOV of the

combined system is exactly $\varphi/2$, i.e. exactly half the normal FOV of the lens camera. Vertical FOV is neither expanded nor contracted by the cone mirror.

Unwarping Algorithm

See Fig. 4. When "unwarping", assuming that the camera is perfectly positioned and lined up, we establish a 2D image polar coordinate system. For a given azimuth and elevation angle in the "unwarped view", the azimuth matches the polar angle directly. The polar radius variable r is related to the elevation as

$$r_p = f_p \tan(\theta - \tfrac{\pi}{2} - \phi) \tag{3}$$

where f_p is the principle distance from viewpoint to image plane of the lens camera in omni-view image pixels (i.e. the pixel unit in the original omni-view image, not the pixel unit in the unwarped image) and is the elevation angle of a point in the 'unwarped' view we want to create (=0 at the horizon, +90 degree upward and –90 degree downward).

Image resolution

It is important to note that the term "resolution" has different definitions in optics[28,29], in CCD and monitor industry and in some computer vision literatures[1,14,17]. In physics, optics and astronomy, the term 'resolution' of an optical system refers to the minimum linear or angular separation between two objects that can be distinguished by the optics. In industry the term 'resolution' has been changed to mean the total number of pixels in two directions and as a whole. In many computer vision literature about omnidirectional sensors the term 'resolution' has been referred to as the ratio of the area or number of pixels on the image plane to the steradian covered. Here we give analysis to both the definition of resolution in traditional sciences and the new computer vision literatures.

To avoid confusion, we call the new definition "Area to Steradian ratio" (bigger is better). This ratio is a function of the distance r of the image point to the image center. The ratio of a small image plane area $d\Lambda$ to its coverage of view steradian *dv* is (Θ :azimuth, ϕ: elevation):

$$\left| d\Lambda / dv \right| = \left| (r\, d\Theta\, dr) / (\cos\phi\, d\Theta\, d\phi) \right| = \left| (\csc\phi\, r\, dr / d\phi) \right| \quad (4)$$

From (3) we have:

$$\left| dr / d\phi \right| = \left| f(1 + \tan^2(\theta_{cone\_tip} - \tfrac{\pi}{2} - \phi)) \right| = \left| f + r^2 / f \right|. \quad (5)$$

Combining (4) and (5) we have:

$$\left| d\Lambda / dv \right| = \left| f \cdot r \cdot \left(1 + (r / f)^2\right) / \cos\phi \right|. \quad (6)$$

For the traditional "resolution" in optics (smaller is better), we really need to consider diffraction effects[28,29]. However, since the pixel sizes in most CCD today are much bigger than the diffraction patterns and are the actual resolution limits we can consider instead the ratio of angle to pixels. In the horizontal direction:

$$360^\circ / (2\pi \cdot r_{pix}). \quad (7)$$

In the vertical direction:

$$1/(f(1+(r/f)^2)) \quad (8)$$

For most CCD cameras, *f* is larger or comparable to *r*, thus (8) is actually near constant over all possible r. Also note that (8) is exactly the same for normal cameras, i.e. the best achievable for similar devices. The cone system is able to view 360 degrees horizontally similar to other omnidirectional camera systems. However, since there is no distortion vertically (to be more precise, on the meridional plane), the vertical FOV is exactly half as that of the lens camera used (like in any other omnidirectional catadioptric system).

Robustness of the SVP condition for cone mirror

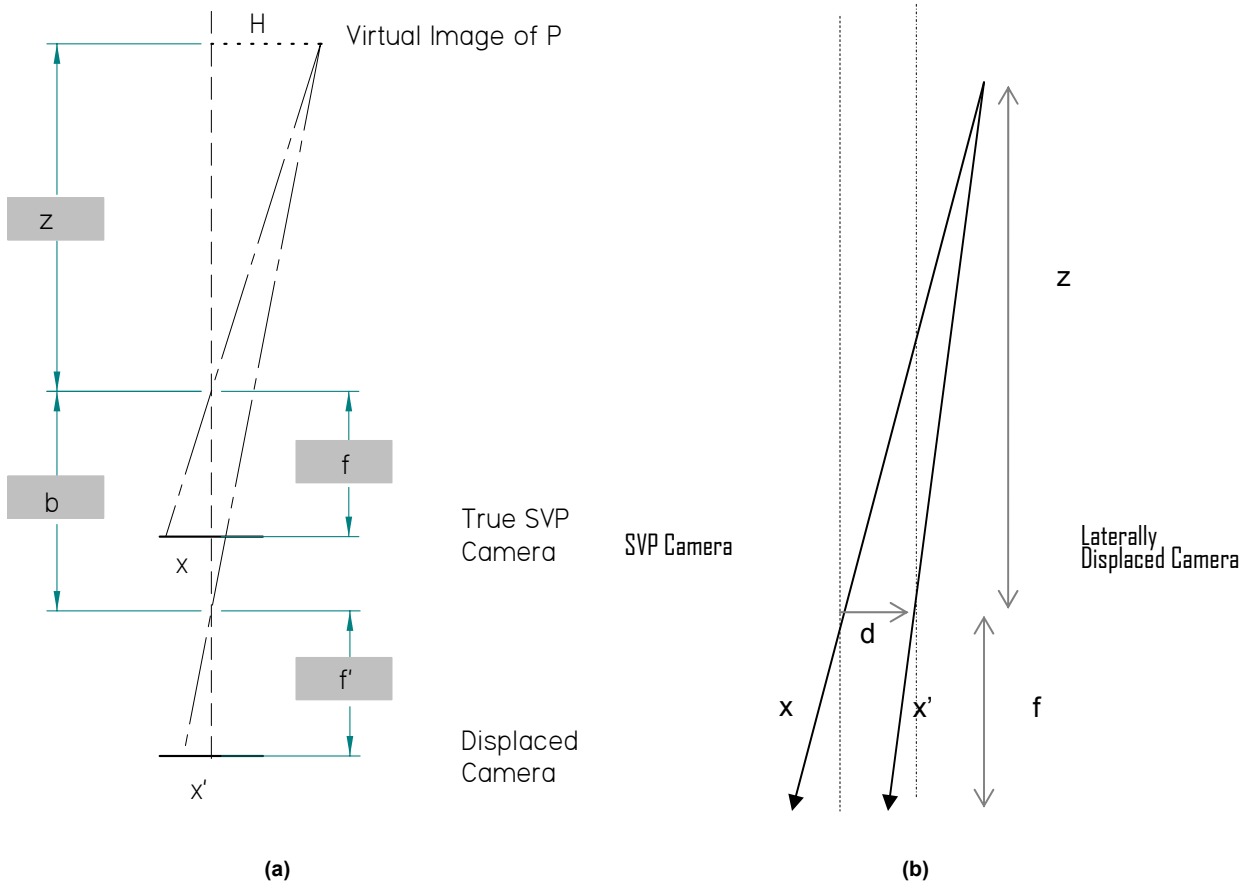

Fig. 5 Deviation from SVP (a) along the optical axis is robust. (b) along the lateral direction is robust.

Despite the best efforts to align the optical components to the ideal positions either by the user or by the manufacturers, there is likely to have some small residual errors left. A very important question about an SVP design is: "How much error in the SVP projection geometry due to misalignments will be detectable?" A very interesting implication from Fig. 1 a is that apart from the aberration caused by the sagittal rays which we will discuss later, the imaging geometry is exactly the same as that of normal cameras. The only difference is that in an SVP cone the "lens camera" is looking at the virtual object. It is well known that for scene at infinity, finite, purely translational movement of the camera has no effects on the pictures. In stereo research this effect

is known in another way, i.e. the parallax effects diminish as the scene gets farther away and vanish completely for scenes at infinity. What these imply is that in practice the SVP condition for the mirror is extremely robust for distant scenes. We can analyze effects of small displacements in two orthogonal directions. In Fig. 5 a, suppose a virtual image point 'P' is projected to position 'x' with the camera ('focal length'=f) positioned at the true SVP. If a camera ('focal length'=f') is placed a distance b away from the ideal SVP along the optical axis, the image position will change to x'. The relationship between x' and x can be expressed as the following:

$$\begin{cases} x/f = H/z \\ x'/f' = H/(z+b) \end{cases} \tag{9}$$

Divide and simplify, we get:

$$(x'/x) = (f'/f)/((b/z)+1) \tag{10}$$

When $f' \cong f$ and z much larger than b, then (10) reduces to $x' \cong x$. Further, similar to the concept of hyper-focal distance (2) we can define "hyper-SVP distance" as the closest distance an object image position exhibits visible position shift due to small deviations of the lens camera viewpoint from the true SVP. From (10), assuming $f' \cong f$ we can write:

$$x - x' = (1-(1/((b/z)+1))) \cdot x \tag{11}$$

Using pixels as the length unit for x and x', if $x - x'$ is smaller than one pixel then the change is practically invisible. Thus the "hyper-SVP" condition can be formulated as:

$$(1-1/((b/z)+1)) \cdot R_{\max} < 1 \tag{12}$$

where $R_{\max}$ is the maximum radial image distance from the center of the cone image in pixels. Typically this can be one half of the shortest side of the image pixel dimension, e.g. $R_{\max}$=240 for 640x480 image. Simplify (12) we get:

$$z > b(R_{\max} - 1) \cong bR_{\max} \tag{13}$$

The "hyper-SVP" distance for cone mirror can thus be estimated as the displacement b times $R_{\max}$, e.g. the hyper-SVP distance for a 640x480 pixel camera displaced 1mm is 240 mm, which is well within the minimum working distance of human eyes (the closest distance for normal adult eyes is 250 mm[28,29]) and many commercial lens camera anyway. Note that a large displacement 'b' will significantly increase the hyper-SVP distance and changes in the omni-view image are likely to be observed. We have utilized large 'b's to construct omnidirectional stereo system in[26].

For small lateral displacements see Fig. 5 b. The relations are:

$$\begin{cases} x / f = H / z \\ x' / f' = (H - d) / z \end{cases} \tag{14}$$

where d can be positive or negative. Assuming $f' \cong f$:

$$|x - x'| = f \cdot |d| / z \tag{15}$$

when z is much larger than $|d|$ then (15) reduces to $x' \cong x$. Assuming the length of the side of one pixel is 's', we have the hyper-SVP distance for lateral displacements as:

$$z > f \cdot |d| / s = f_{pix} \cdot |d| \tag{16}$$

where f_{pix} is the projection 'focal length' in units of pixels. With 640x480 pixels 2/3" CCD (s=0.014 mm) and f=6mm lens, the hyper-SVP distance for 1mm lateral displacement is about 436 mm, somewhat longer than that in the longitudinal direction, but still inside the minimum working distance of many lens cameras. The criteria for determining hyper-SVP distance for changes less than one pixel can be further relaxed for some applications.

As long as there is no tilting, the SVP can be practically maintained for far scenes with pure translations without any recalibration. The robustness is maintained for scenes closer in

longitudinal displacement than in the lateral displacements. This is much more tolerant than the hyperbolic mirror and close to the freedom allowed in the parabolic mirror. The orthographic projection in parabolic mirror is still better in that its flexibility is maintained even for close scenes. In terms of tilting, the cone mirror has the same tolerance as the hyperbolic mirror in that SVP is still maintained, but the projection needs recalibration.

ABERRATION ANALYSIS

Imaging Characteristics of the Cone Mirror

Pin-hole model based analysis shows that the imaging characteristics of the SVP cone are perfect. However, in practice the sagittal rays cannot be ignored and they introduce visible blurring not predictable by the pin-hole model. The blur is more severe toward the center of the image. Below we analyze the effects of aberration and also point out ways to reduce the aberration. For any given world point not on the optical axis the plane that contains both the object point and the optical axis is called a meridional plane. A ray lying on the meridional plane is called a meridional ray. The meridional ray that passes through the center of the entrance pupil is called the chief ray and for each straight line segment of the chief ray the plane that contains that segment of chief ray and perpendicular to the meridional plane is called the sagittal plane. See Fig. 6. The cross section of the cone mirror at the meridional plane is always a straight line. Just like the plane mirror there is no aberration at all for meridional rays. The extension of any meridional ray reflected by the cone mirror surface will intersect at the same point, forming a perfect virtual image.

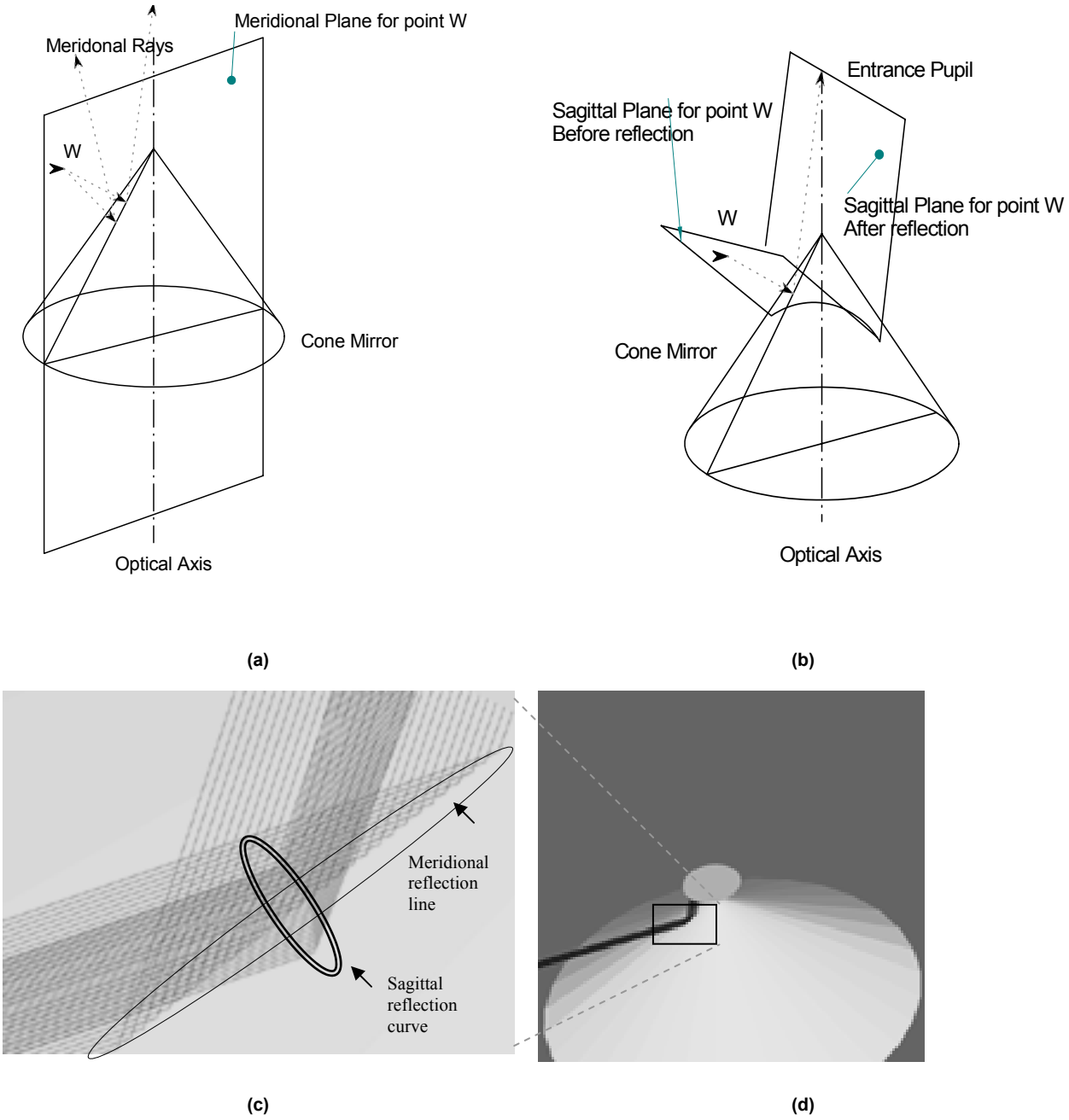

Fig. 6 Meridional plane (a) and Sagittal plane (b) for world point W and the cone mirror system. (c) Reflection pattern at meridional plane and sagittal plane at the cone surface. (d) Overview. (c) and (d) are actual ray trace result by Zemax®.

The situation on the sagittal plane for a cone mirror is quite different. Just like any other convex surface of revolution mirrors, the surface of the cone mirror is composed of concentric circles with varying radii. The intersection of a sagittal plane with the surface of revolution mirror will be a curve and the surface normals along the intersection curve will in general not lie

on the same plane. For a cone mirror, the intersection curve with a sagittal plane will be a conic section curve. Because of this curve of intersection, we will see local diverging effects even when the aperture size approaches zero. This gives rise to spherical aberration in the sagittal plane[2]. When the aperture is large, slight coma can be observed. The most important effect, however, is that the divergence of rays causes the sagittal rays to form a sagittal virtual image that is closer than the meridional virtual image. The meridional virtual image is a perfect image that has almost the same object distance as the original real object. This disparity of focusing becomes more pronounced closer to the tip of the cone because the curvature of the sagittal curve approaches infinity at the tip of the cone while the curvature of the meridional mirror cross section remains at zero. Fig. 6 c and d is an example of the reflection patterns of meridional rays and saggital rays at the cone surface. Notice that the reflection points of all the meridional planes form a straight line while those of sagittal rays form a curve. At the meridional image plane, the sagittal imperfection shows up as line like patterns but the centroid of the blur pattern remains at the SVP position.

The difference of image qualities between the sagittal and meridional planes of the cone mirror indicates the presence of astigmatism. The most prominent visual effects of astigmatism are the existence of two distinct best focus settings for meridional and sagittal rays respectively. When the image plane is placed at the meridional focus the image will be perfectly focused along the meridional plane but blurred in the orthogonal direction. However, as long as the blur radius is not too large compared to the size of the smallest sensing unit (for CCDs this means the size of its physical pixels) then the effects can be practically invisible on the resulting image. Thus we are going to trace a significant number of rays coming from a world point until they reach the imaging plane and see the resulting radii of the scatter patterns, called “spot diagrams”.

Optical Ray Tracing

Without going into wave optics, the most realistic way to trace all the rays collected by the optical system is to use law of reflection and refraction at the exact surface locations. However that requires the knowledge of the exact shapes and positions of all the optical surfaces and the detailed material properties of each component. These data are usually not available for off-the-shelf video lens. Thus we will only give an example of real system using this most detailed ray tracing method[28,29].

Like Baker and Nayar[1], we do not consider diffraction effects here. However, we do show that when this simplification is reasonable. The ray aberration is much bigger than diffraction pattern in most cases. We assume the CCD is 2/3" format (8.8 mm by 6.6 mm effective chip area) with pixel width about 14 microns. Image qualities at 4 image positions (fields): (1) 3.3 mm (2) 2.2 mm (3) 1.6 mm (4) 0.8 mm from the center of CCD chip are shown representing the image qualities from the edge of an omni-view picture toward the center of the picture. The standard system is modeled after our prototype system with cone tip angle 107 degree and lens focal length 6 mm. The front focal point serves as the single viewpoint of the lens camera. We use 250 mm as close-in distance and 50000 mm as far distance. A typical spot diagram results are shown in Fig. 11. The RMS (Root Mean Square) radius of the "cloud of points" is defined to be the RMS of distances between each image point and the centroid of all the points calculated. All optical ray tracing numerical calculations have been done with the help of ZEMAX® [31], a professional optical design CAD software.

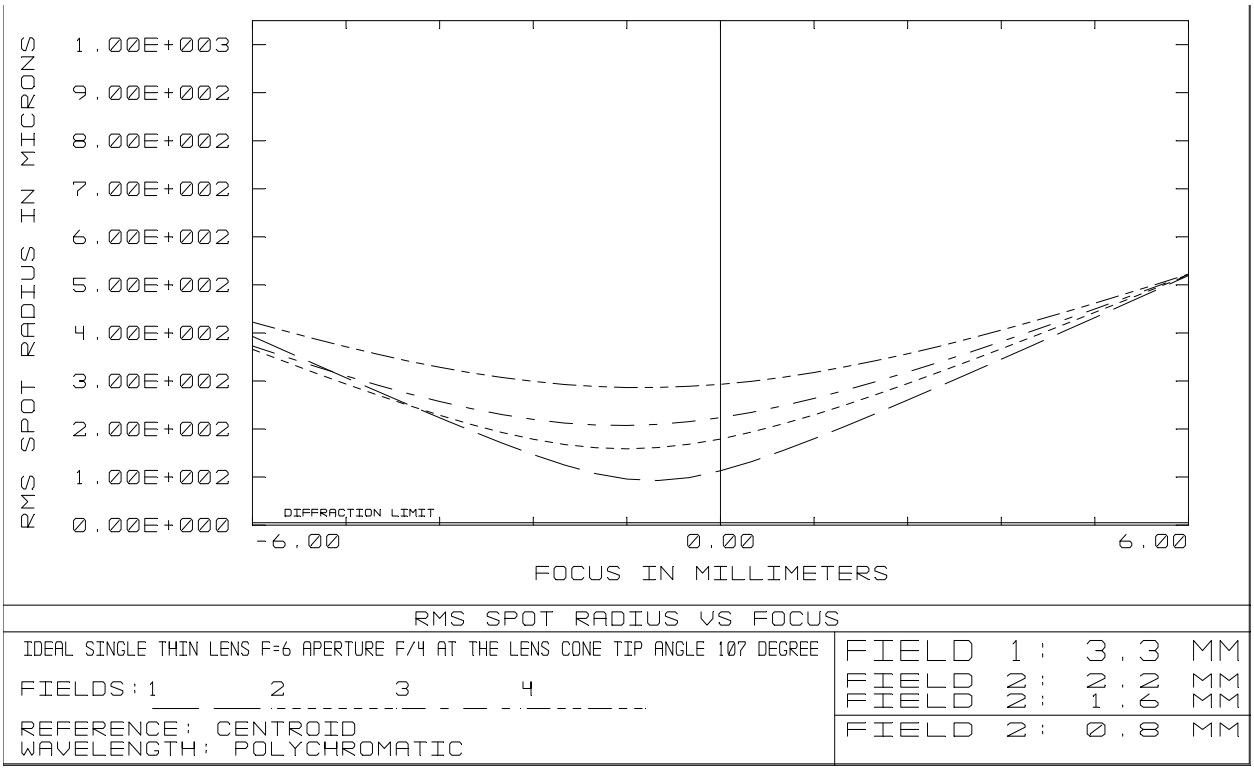

Fig. 7 Uncorrected System Focusing plot

With a single ideal lens whose diameter serves as the aperture stop at F/4, the variation of RMS radius of the image of a point object versus the distance of image plane distance is shown in Fig. 7. The image plane distance shown on the X-axis is centered on the paraxial image plane distance determined by (1) with negative values indicating farther away from the lens surface. Here all fields reach best focus at about -0.8~-0.9 mm away from the paraxial focus. This means that overall field curvature aberration is small. The less than 1 mm focus position shift from paraxial focus has the effect of slightly enlarging the image if we focus at that position. The spot size is much larger than diffraction limits so it is reasonable to ignore diffraction effects.

In Fig. 7 the image quality differs significantly at different image positions and that the spot sizes are large compared to the pixel size. The source of these problems is astigmatism, as shown in Fig. 8. The meridional rays are all perfectly focused at the paraxial focus (only differs by about 0.004 mm) with spot sizes (6~16 μm) comparable to the pixel size (14 μm). The best

spot sizes for the sagittal rays are also comparable to the pixel size but the best focus position between fields varies significantly, indicating large sagittal field curvature. Practically all real optical systems have some kinds of aberration. We just need to find the proper system setup so that our sensors do not see the unwanted effects or in a form we know how to correct them. In fact all catadioptric omni-cam systems deliberately introduce large distortion (also a kind of aberration) in order to get large FOV. We did the same analysis for object distance at 5000 mm and 50000 mm but found that the results are very similar, with only minute variations in numbers, so we show only plots for object distance at 250 mm here.

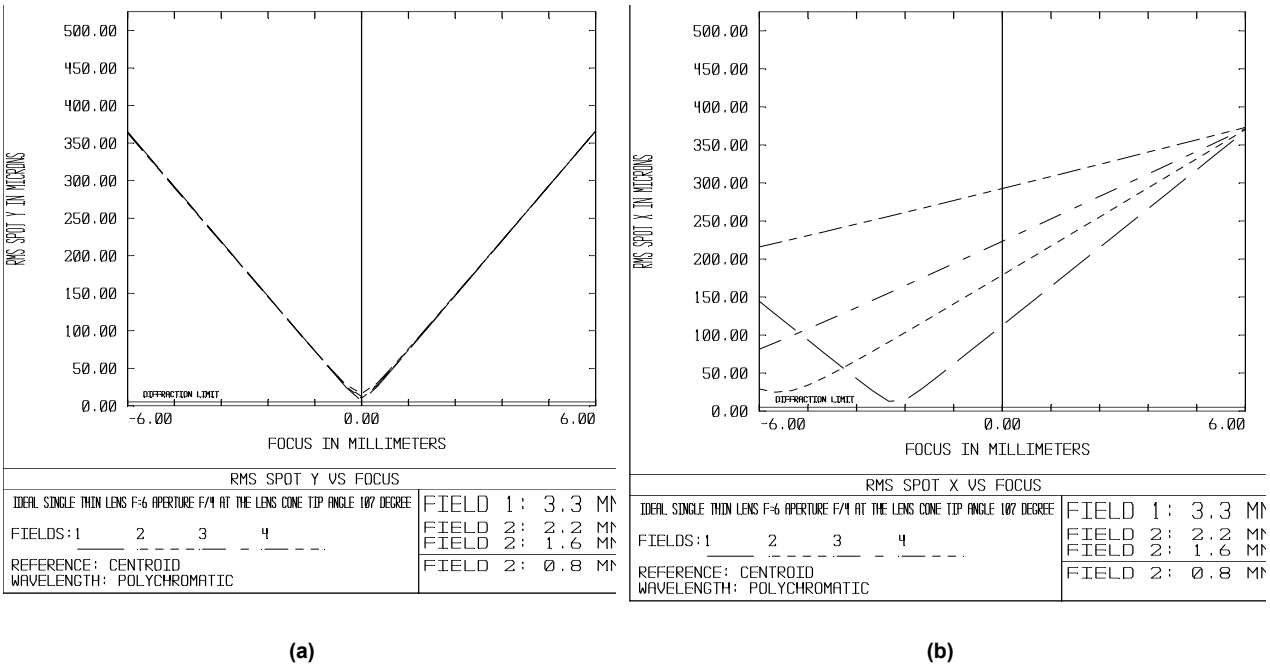

(a) (b)

Fig. 8 Focusing diagrams of meridional (a) and sagittal (b) rays.

MINIMIZING ABERRATION EFFECTS

The aberration analysis showed significant astigmatism for cone mirror. However that does not mean we can not minimize the effects by adjusting several optical components of the system. In fact most real optical systems have intrinsic aberrations, e.g. a single element spherical lens always has spherical aberration[28,29]. Having inherent aberration does not render an optical

component useless. By combining other components the total system aberration can often be reduced to acceptable level. We show below how we can change the total system aberration by changing the parameters in the lens components.

Changing Stop Size and thus F/#

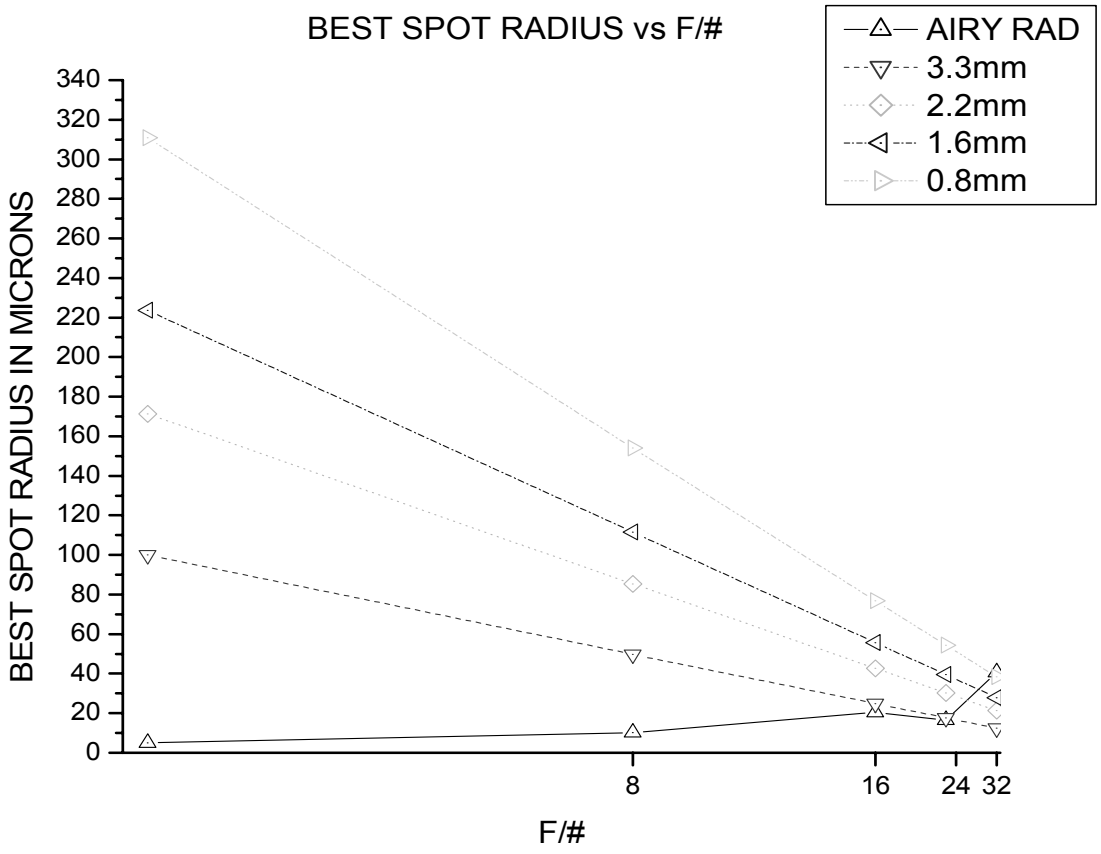

Fig. 9 F/# change reduce best focus spot sizes.

We first change the aperture size (and thus F/#) without moving the aperture stop. The best focus positions are almost unaffected, with focus position shifts in the order of 0.001 mm so we do not plot focus shift diagrams again, the shapes will look very similar to Fig. 7 and Fig. 8. However we do see significant improvement in best spot radius. Fig. 9 shows that the best focus spot sizes in all field positions are reduced significantly. The X-axis scale is the reciprocal of F/# so we see that the best focus spot radii change linearly with the radius of aperture stop. We also plot the

radius of Airy diffraction disk radius. For F/# from 16 to 22 the edge of image (3.3 mm) will reach diffraction limit.

Changing the Stop Position while Maintaining F/#

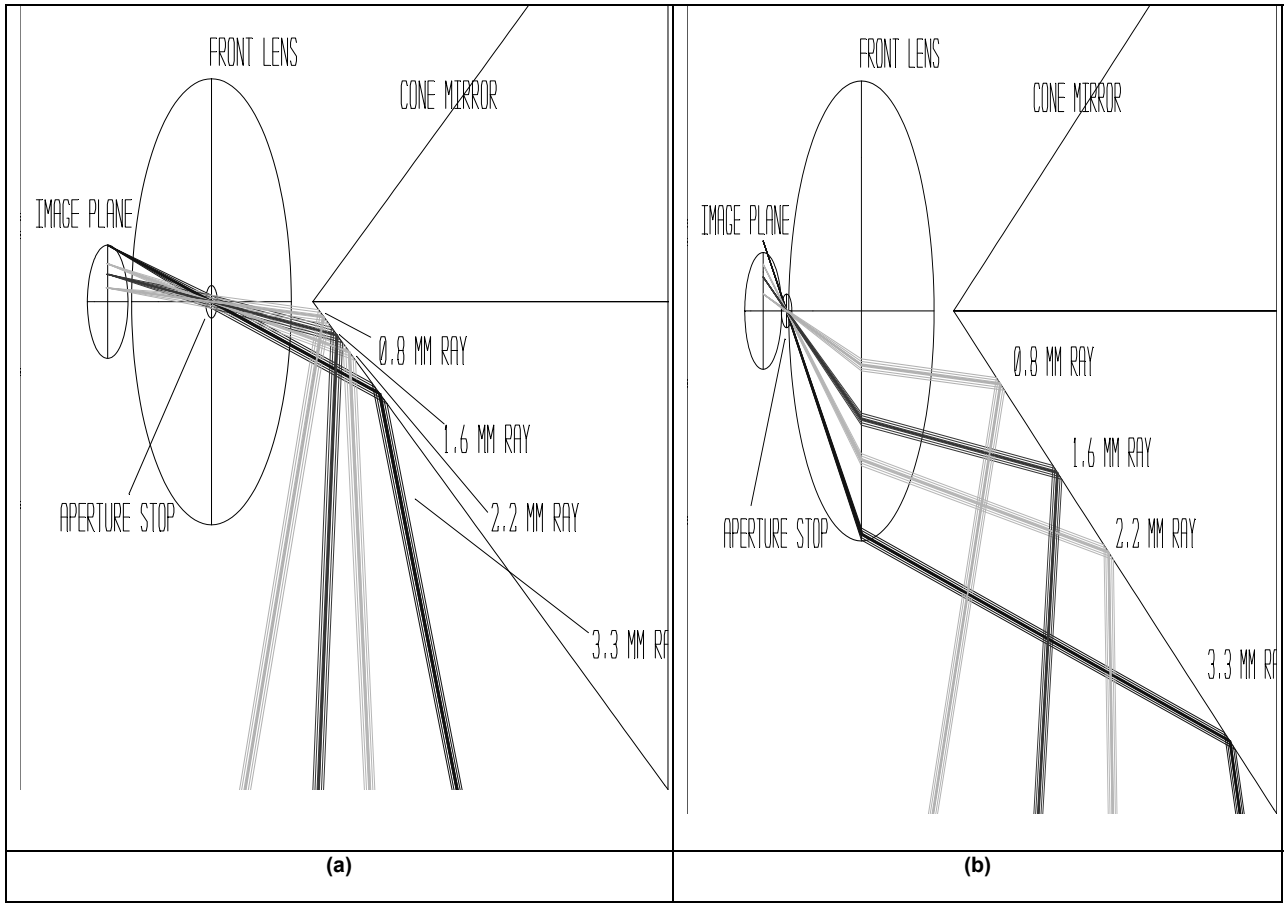

Fig. 10 Aperture stop placed away from the front lens improves image quality. (a) Placing the stop at the lens the rays are reflected near the tip of the cone where the surface curvature difference is greatest. (b) Placing the stop behind the front lens selects rays reflected at mirror surface points farther away from the tip. Note that the image positions do not change when stop position is changed. Both graph here is F/#=8.

Closing the aperture helps improve the image quality but not well enough. Most real CCTV lenses have their aperture stop behind some lens elements. That makes the entrance pupil much farther away from the cone mirror, which in turn chooses better chief rays that are reflected farther away from the tip of the cone. See Fig. 10. The best focus image spot sizes are indeed improved significantly. If the F/# remains fixed, the farther away the aperture stop position is from the lens, the better the image. The trend diagram has similar general shape like Fig. 9, with

the X-axis replaced by the entrance pupil position. However the farthest distance we can move the stop away from the front lens is limited by vignetting. In Fig. 10 we see that as the aperture stop moves farther away the points where the rays enter the front lens also move toward the outer edge of the lens. In this example the farthest distance we can move the stop without having vignetting at the edge of the image (3.3 mm field) is about 4.865 mm. At this setting the best focus within diffraction limit is achieved at F/8.

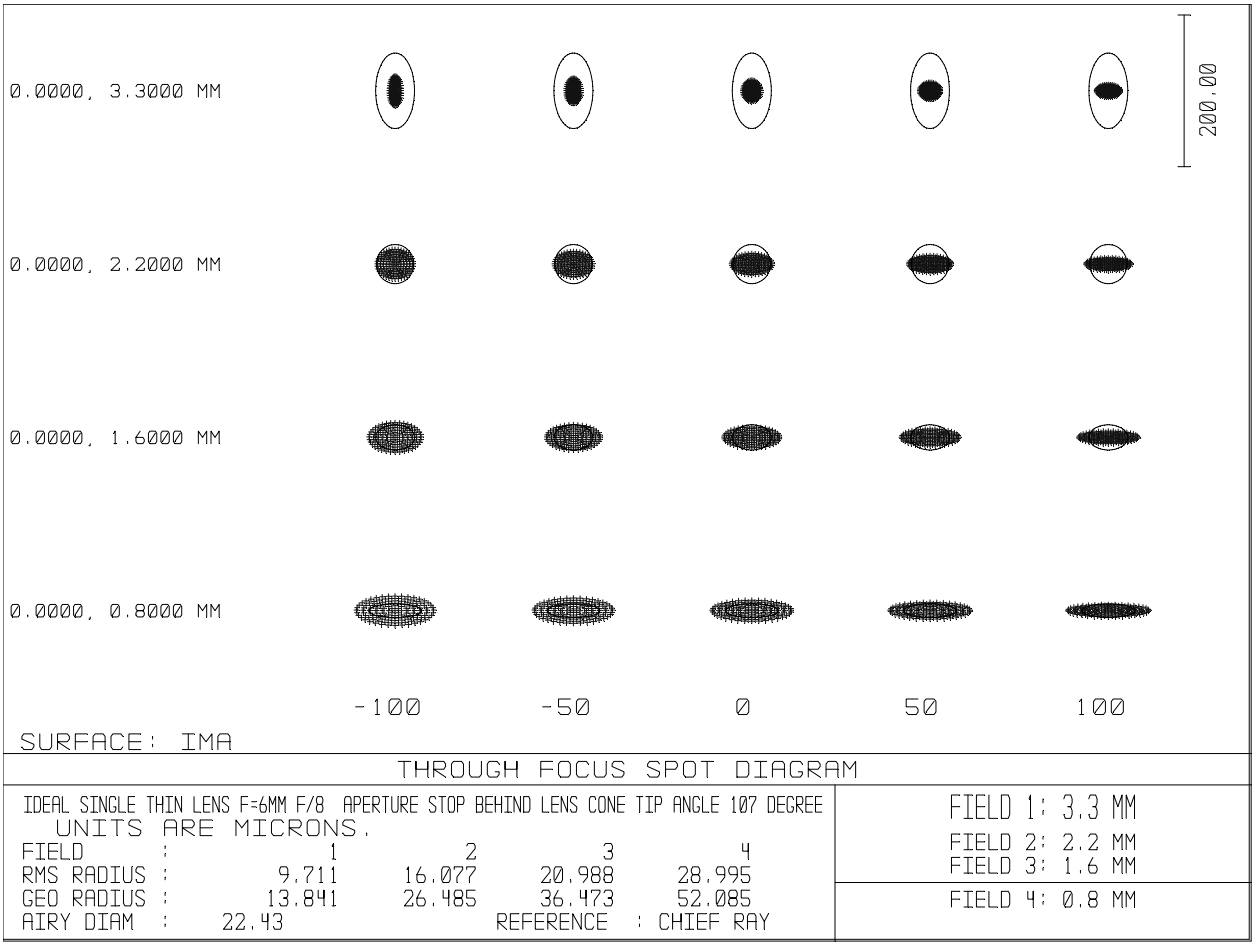

Fig. 11 The best focus that is diffraction limited and without vignetting is achieved at F/8 and stop 4.865 mm behind front lens for our test system.

See Fig. 11, the center column is the spot pattern for all 4 image positions to show that they can achieve the best focus almost simultaneously. The other columns show the change of spot patterns with tiny movement of image plane (± 50 and 100 microns). The circles are

estimates of Airy disc diameters. Here we achieve smaller RMS radius with larger aperture than fixing the aperture stop at the lens surface, compare Fig. 9.

Changing mirror shapes

From the same reasoning in Fig. 10, we can see that the sharper the tip angle of the cone, the farther away the point of reflection will be and also the horizontal curvature of the mirror at the point of reflection will be smaller. Thus the smaller the tip angle (of the cone mirror) the better. However, due to practical considerations like the range of FOV, typical tip angle of the cone mirror would be near 90°. The improvement from tip angle 114° to tip angle 90° is the reduction of RMS radius at 3.3 mm from 14.6 μm to 9.8 μm.

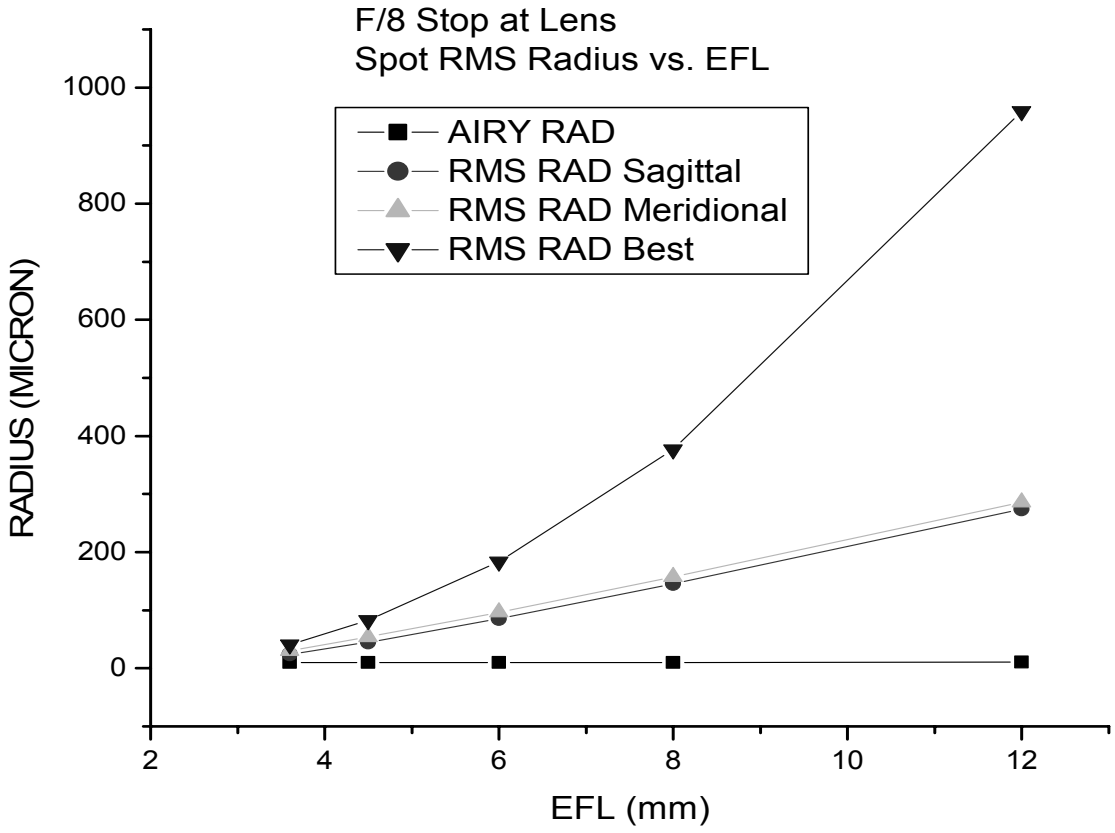

Fig. 12 RMS spot radius (image position 2.2 mm from the center of CCD) vs. lens EFL (F/# fixed at F/8, aperture stop at lens, SVP at object side focus). Sagittal, Meridional and Best indicates focus settings.

Changing Focal Length while Maintaining F/#

Changing focal length changes magnification. Magnification magnifies the aberration patterns. Thus the best spot size changes linearly with the focal length. The shorter focal length will produce smaller aberration patterns and thus better image quality. See Fig. 12. The divergence of "best" (overall) curve indicates large astigmatism at long focal length so should be avoided.

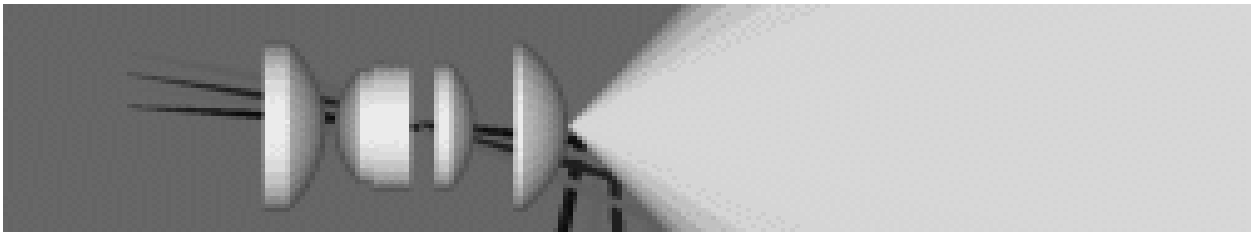

(a)

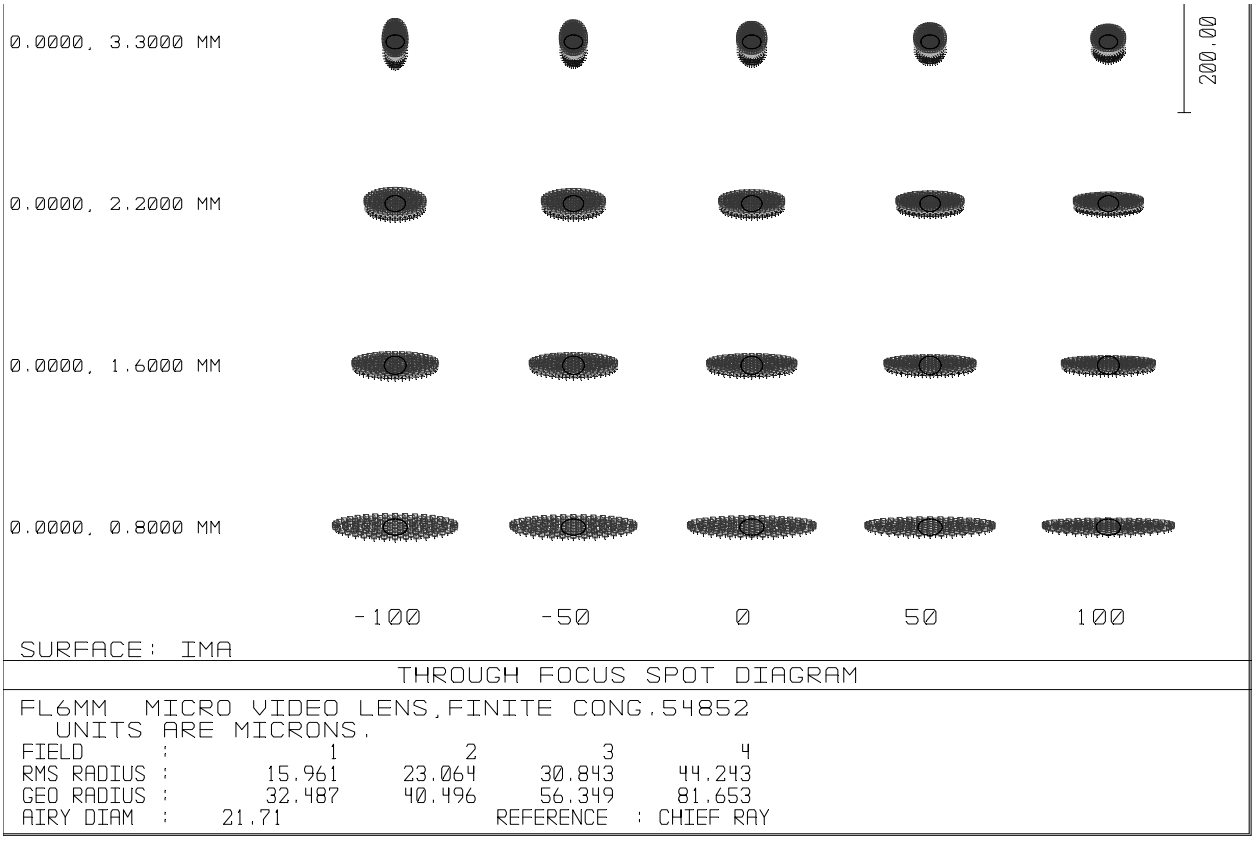

(b)

Fig. 13 (a) Real lens ray-tracing using Edmund Optics 6 mm lens, stock #54852. (b) Real lens ray tracing results adjusted to the optimum configuration. Here we use F/16 as a compromise before the diffraction effects grow too large.

Real Lens Example

Real CCTV lenses have several lens elements with aperture behind or between them. The exact composition is usually not available for the general public. Edmund Industrial Optics® offers to give us the complete prescription of its 6 mm lens, stock #54852, so we can use the exact Snell's law of refraction to do ray tracing, see Fig. 13. Note that Fig. 13 looks similar to Fig. 11, indicating the validity of our general approach.

FREQUENCY RESPONSE ANALYSIS

Many catadioptric omnidirectional sensors today are used for machine vision and robotic research and applications. For many computer vision algorithms the most important requirement for image quality is "How well does it preserve features in the scene?". In most cases the features in the scene corresponds to high frequency patterns in the images.

Frequency Response of Catadioptric Optics

From Fourier transform theory we know that all image patterns can be regarded as combinations of periodic sinusoidal patterns. From previous analysis we already know how each single point is spread out by the catadioptrics of the cone omnidirectional sensor. Since lines are made up of points along a given direction, we can compute the line spread function using the point spread diagram obtained in our ray tracing analysis.

Given a point spread pattern, if we divide the area along the direction of the line direction we are interested in into tiny narrow strip intervals Δx or Δy and count the number of ray hitting the image plane, we can construct a Line Spread Function (LSF) for this point spread pattern along the particular direction. See Fig. 14. The value of LSF(x) is the relative number of ray hit inside the narrow strip interval of width Δx centered on the position x. This function represents how an

ideal perspective projection line on the image plane will be spread out by the real optical system. Similarly, the edge response can be obtained by counting the ray hit points, only that we count the total points to the right or left of current position instead of counting the number of points inside the immediate narrow strip area.

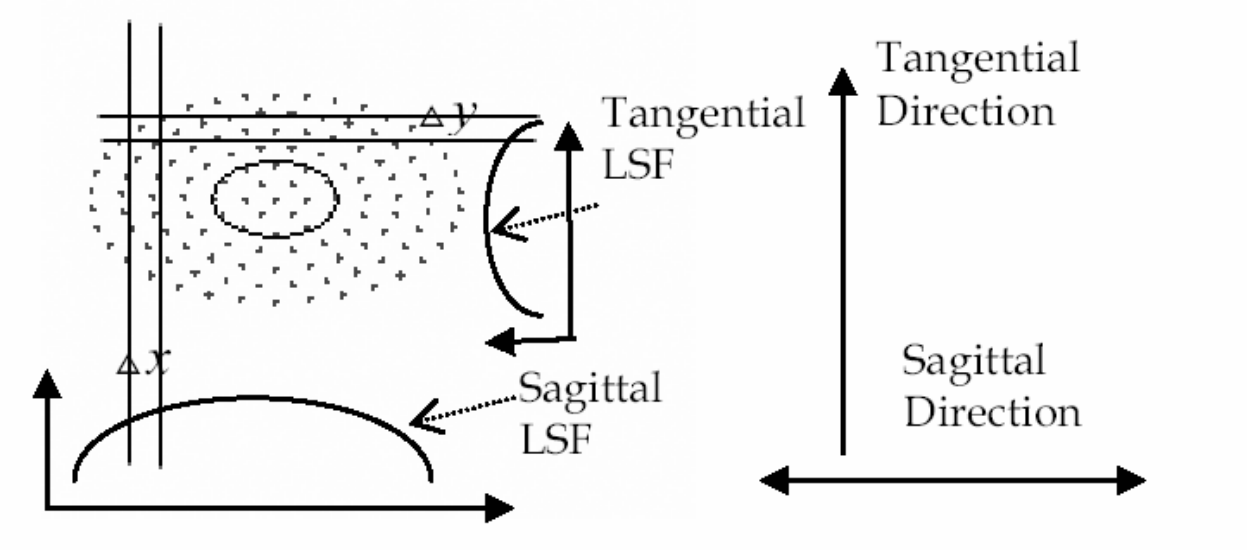

Fig. 14 LSF (Line Spread Function) along tangential and sagittal directions.

Once we have LSF, then the frequency response to a sinusoidal pattern with gain level U, amplitude A and frequency υ can be computed by convolving the sinusoidal function with the LSF. From Fourier transform theory we know that convolution in space domain equals multiplication in the frequency domain. Since the Fourier transform of the sinusoidal pattern with frequency υ is always two symmetric dots at +υ and –υ we know that the result of convolution will still be a sinusoidal function of the same frequency. However, the amplitude A and its phase may be different. If we define the sinusoidal pattern *G(x)* as follows:

$$G(x) = U + A\cos(2\pi\upsilon x) \tag{17}$$

We can define F(x) as the convolution of *G(x)* and LSF(x) normalized by the total brightness of the line pattern:

$$F(x) = \frac{\int LSF(\delta)G(x-\delta)d\delta}{\int LSF(\delta)d\delta} \tag{18}$$

We have:

$$\begin{aligned} F(x) &= U + A\left|T(\upsilon)\right|\cos(2\pi\upsilon x - \phi) \\ &= U + AT_c(\upsilon)\cos(2\pi\upsilon x - \phi) + AT_s(\upsilon)\sin(2\pi\upsilon x - \phi) \end{aligned} \tag{19}$$

where:

$$\left|T(\upsilon)\right| = \sqrt{T_c(\upsilon)^2 + T_s(\upsilon)^2} \tag{20}$$

$$T_c(\upsilon) = \frac{\int LSF(\delta)\cos(2\pi\upsilon\delta)d\delta}{\int LSF(\delta)d\delta},$$

$$T_s(\upsilon) = \frac{\int LSF(\delta)\sin(2\pi\upsilon\delta)d\delta}{\int LSF(\delta)d\delta}, \tag{21}$$

$$\tan\phi = \frac{T_s(\upsilon)}{T_c(\upsilon)} \tag{22}$$

If we define the modulation of the periodic pattern as:

$$M = \frac{Max - Min}{Max + Min} \tag{23}$$

The original periodic function before convolution has modulation M_o:

$$M_o = \frac{U + A - (U - A)}{U + A + U - A} = \frac{A}{U} \tag{24}$$

The actual image pattern after "degradation" from the optics will be M_i:

$$M_i = \frac{A}{U}\left|T(\upsilon)\right| = M_o\left|T(\upsilon)\right| \tag{25}$$

If we know such function |T(υ)| at every frequency then from Fourier transform theory we also know how the optics will distort any given pattern. This function is so useful it is called MTF (Modulation Transform Function) in optical literatures[28,29]:

$$MTF(\upsilon) = \left|T(\upsilon)\right| = \frac{M_i}{M_o} \tag{26}$$

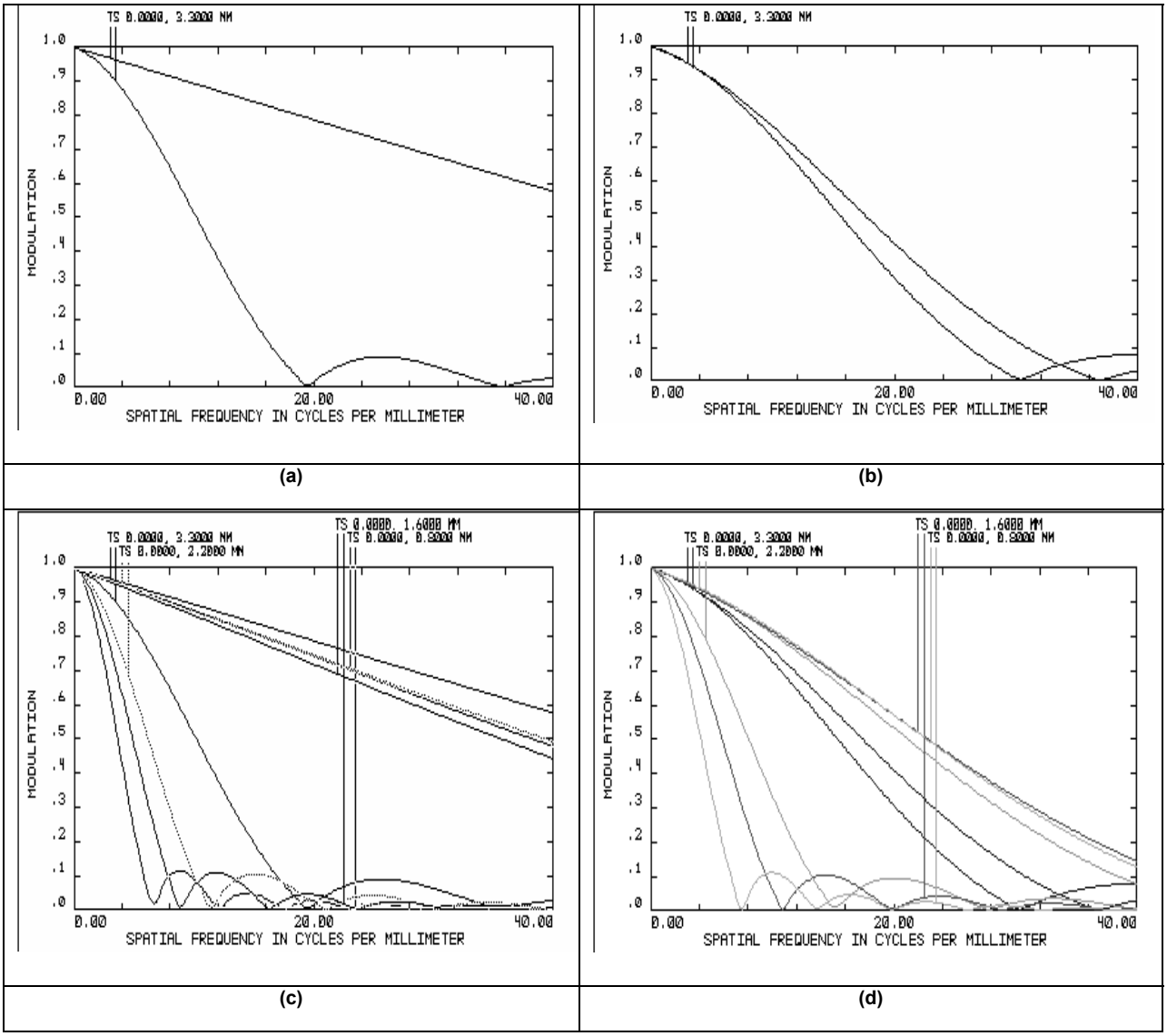

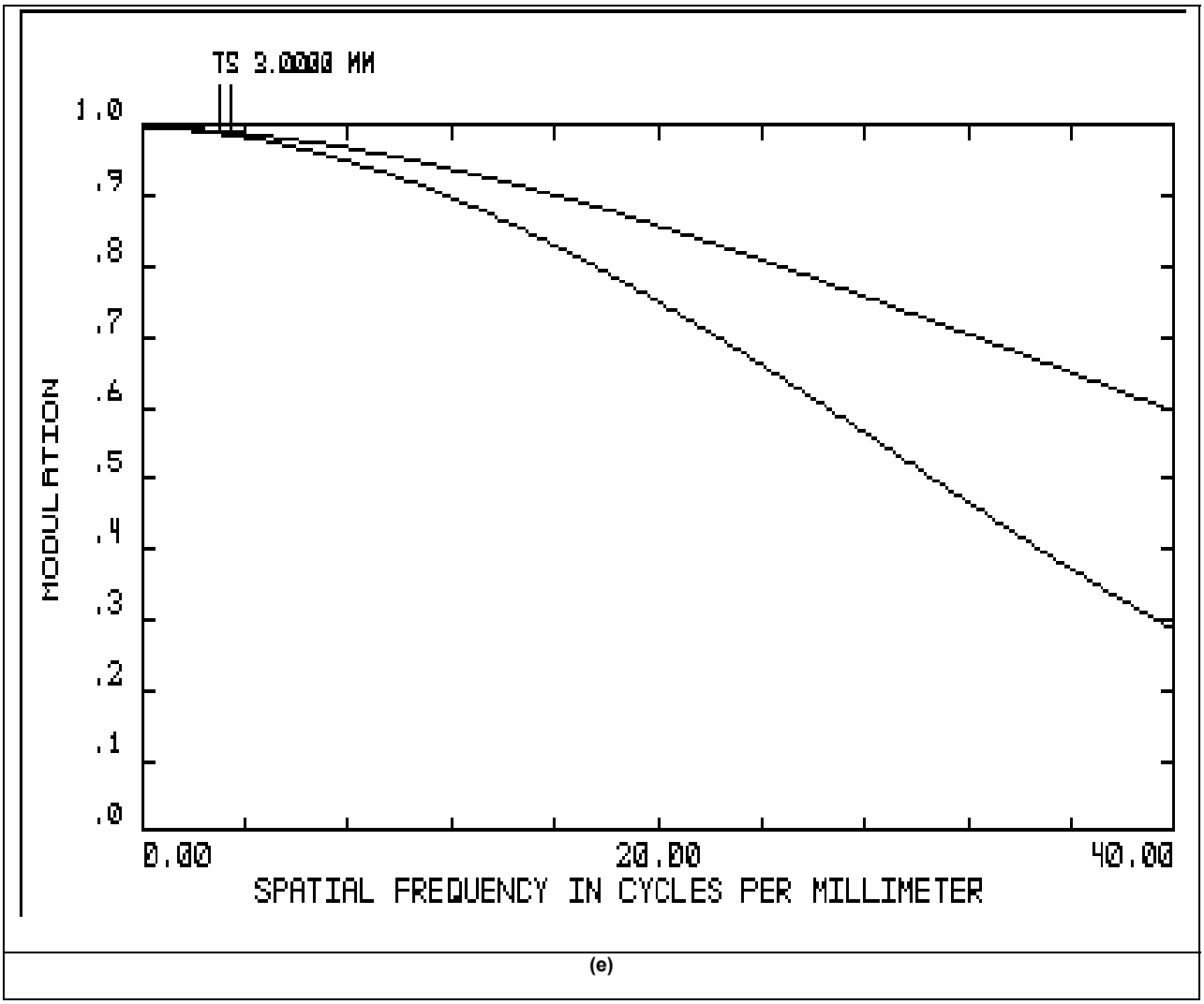

Fig. 15 T: Tangential, S: Sagittal. (a) MTF curves of meridional focus at the rim of the image. (b) MTF curves of best focus at the rim of the image. (c) MTF curves of 4 image positions at the meridional focus. (d) MTF curves of 4 image positions at the best focus. (e) MTF of the normal lens (Edmund #54852).

The phase change mentioned in (19) and (22) can be important when the LSF is not symmetric around the center. For symmetric LSF the phase change is always zero. Note that when we use the point spread plot calculated purely using geometric optics, the MTF does not take into account the diffraction effects. This is fine if aberrations are small. According the Rayleigh criteria the aberration is considered small if the optical path difference or wave front distortion is close to $\frac{\lambda}{4}$, in our example system the smallest optical path difference occurs at the rim of the

image and it is bigger than λ (we use λ= 0.58756180 μm). Thus it is safe for us to use the geometric LSF here[28,29].

Fig. 15 shows the MTF of the best configuration we found in the last section. Compare the tangential MTF at Fig. 15 a with that of Fig. 15 e, we see that the tangential MTF of SVP cone is just as good as that of a normal perspective camera. This is a numerical validation of our theoretical prediction that the meridional imaging of SVP cone is perfect. However we can see that at the same time the sagittal MTF is much worse, due to astigmatism. At the best focus we sacrifice some meridional performance in exchange for a siginificant improvement in sagittal MTF. In practice, using the best focus may give a more pleasing overall picture quality. The meridional focus may still be useful for certain applications that needs fine details only in the meridional direction.

Frequency Response of the Film or CCD

The MTF curves of hyperbolic and parabolic mirrors in general look better than SVP cone if one takes the spot diagram in[1] and do the same MTF analysis. Fig. 16 a is the MTF curves for an SVP parabolic omni-cam in our lab. However, as we will see in the experiments, SVP cone omni-cams actually preserve more fine details in the unwarped images for the same object pictured at the same distance. The reason is that the spatial frequency used in MTF analysis is calculated at the image plane, not on the object surface. Because other curved surface mirrors have much higher meridional FOV, they must have a much smaller meridional angular magnification. The same object details imaged by other curved mirrors will have higher image plane spatial frequencies. Due to digitization, there is a maximum cut-off frequency that can be resolved by a CCD chip. For our 2/3" 640x480 CCD, the cut off frequency on the image plane is about 40 line pairs/mm (a more practical limit, considering the Nyquist frequency, is 20 line

pairs /mm). The problem with meridionally curved surface mirrors are that many object details will be imaged with higher frequency than the cut-off frequency of CCD and completely disappear. For comparison with SVP cone in terms of the meridional object pattern frequency, the MTF curve for SVP parabolic should multiply the frequency scale by the ratio of cone meridional lateral/angular magnification to that of the parabolic mirror. This factor is about 5 in our experiments. Fig. 16 b is the rescaled Fig. 16 a. Note that not only does the rescaled parabolic MTF shows up inferior compared to the cone MTF, but the hatched region are all above the 40 lp/mm cut-off frequency and will never show up in real pictures. E.g. if an object pattern shows up 40 line pairs per mm on the CCD chip of an SVP cone, the same pattern would show up on the CCD chip of an SVP parabolic as 40x5=200 line pairs per mm and will not be discernable.

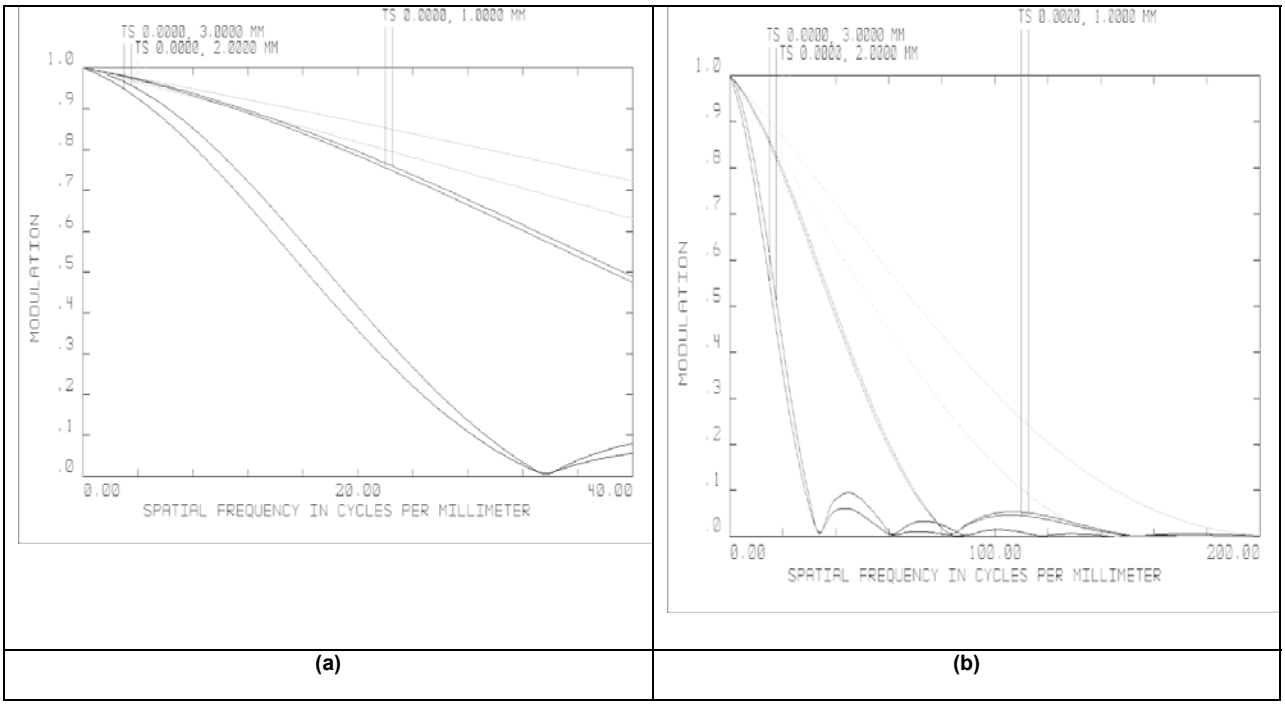

(a) (b)

Fig. 16 (a) SVP parabolic mirror MTF at the image plane. (b) The same MTF adjusted for original object spatial frequency.

Experiments

In our previous works[4,6] we have shown experiment results proving that an SVP cone omnidirectional imaging sensor setup can indeed form images properly and can be unwarped properly. We have also demonstrated the higher angular resolution of the cone based omnicam system as compared to existing systems that are based on meridionally curved mirrors. This work is primarily a theoretical analysis but we do have done a few experiments to verify some of our new theoretical predictions.

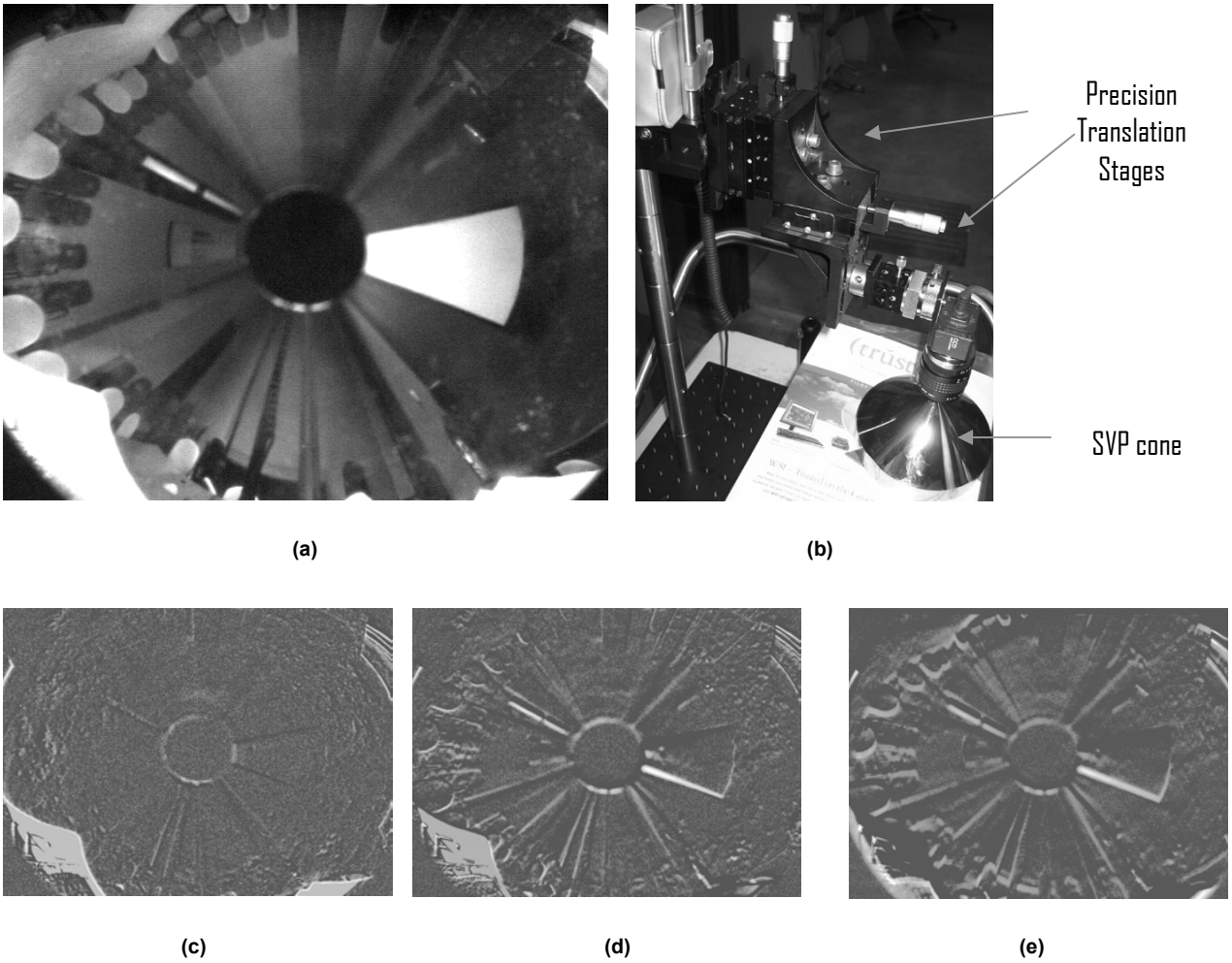

Fig. 17 Robustness tests. (a) Precise SVP image.(b) Experiment setup. (c) Subtraction image of image with camera moved .025" back minus the SVP image. (d) Subtraction image of the image taken with camera .025" to the bottom side with the SVP image. (e) Subtraction result of a digitally shifted 10 pixels down image minus the SVP image. All subtraction images are histogram enhanced, otherwise looks almost all black.

To demonstrate the robustness of the SVP condition of cone mirrors, we use setup shown in Fig. 17 a. The translation stage is THORLABS MT3, capable of 0.025" per revolution of the knob

and 0.001" per graduation. We tried .025" movement in lateral (down direction in the image frame) and longitudinal (back along the optical axis) directions. The images taken at slightly decentered positions are then subtracted with the accurate SVP image. The results are shown on Fig. 17 c~e. The cone omni-cam is placed at the center of a big conference room. The white object on the bottom left and right of the omni-view is a paper on the desk very close to the omni-cam. As predicted by (13) and (16), very little change is visible and only for objects very close or near the edge of the omni-view. We used both edge based and correlation based method to find the scene displacements between two images. The results are summarized in Table 1. Only edge based model finder reports 3.18 pixels displacement in lateral decentering. Longitudinal deviation from SVP causes virtually no effects. As predicted, the SVP condition is more robust against longitudinal displacements than lateral displacements. For comparison, Fig. 17 e is the subtraction between a digitally displaced SVP image (10 pixels down) with the original SVP image.

Table 1 The data format is (X displacement, Y displacement)

	Longitudinal	Lateral
Edge based	(+.007, +.20)	(-.34, -3.18)
Correlation based	(+.48, +.40)	(+.48, -.18)

For testing outdoor performance and focusing properties, we used a CASIO QV-2000UX digital camera (1/2" CCD, f=6.5mm) with different optical settings. This camera allows full manual control (an undocumented feature) for aperture, shutter speed and focal length (3X ZOOM). We can partly compensate for small apertures by using longer exposure time. For day outdoor scenes lighting conditions are sufficient with NTSC frame rate exposure time (1/30 sec) or less. We took a picture at every adjustable F/# setting and we always tried to focus the picture

to the best of our abilities. Since the meridional focus has spot sizes only slightly larger than the best focus and its focus position is close to the best focus position, we always try to focus to the meridional focus. The meridional focus is easily recognized because we can see only a concentric blur (around the image center) but no radial blur. Another nice property is that the meridional focus position does not move when one changes the aperture setting. Thus the best way to focus is to open up the aperture to the fastest setting allowed, adjust focus to remove all the radial blurs, and then close down the aperture to the desired value.

As predicted we cannot focus well if the aperture is wide open. Fig. 18 a is an example of a picture taken at F/2. From the center of the image to the about half way to the edge the blur is significant. From the middle to the edge of the image the blur is less significant but is still not sharp. In contrast, Fig. 18 taken with F/10, 1/30 sec shows no visible blur in most of the image except when very close to the image center. It shows that it is possible to take good quality SVP cone omnidirectional video because 1/30 second is the maximum normal exposure time for an NTSC format video frame. Fig. 18 c and d are unwarped from portions of the Fig. 18 b. They demonstrate that fairly good quality unwarped images can be obtained.

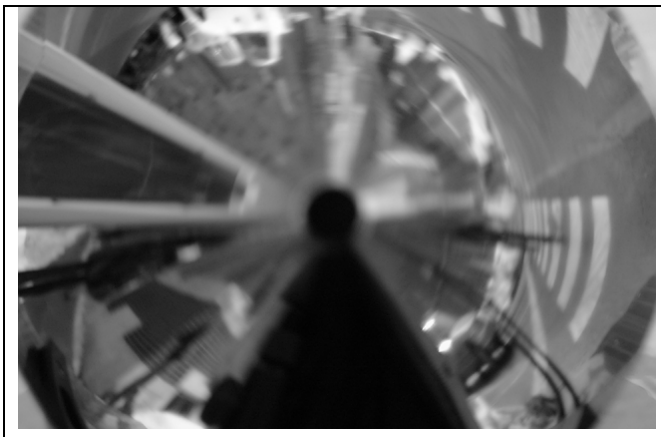

(a)

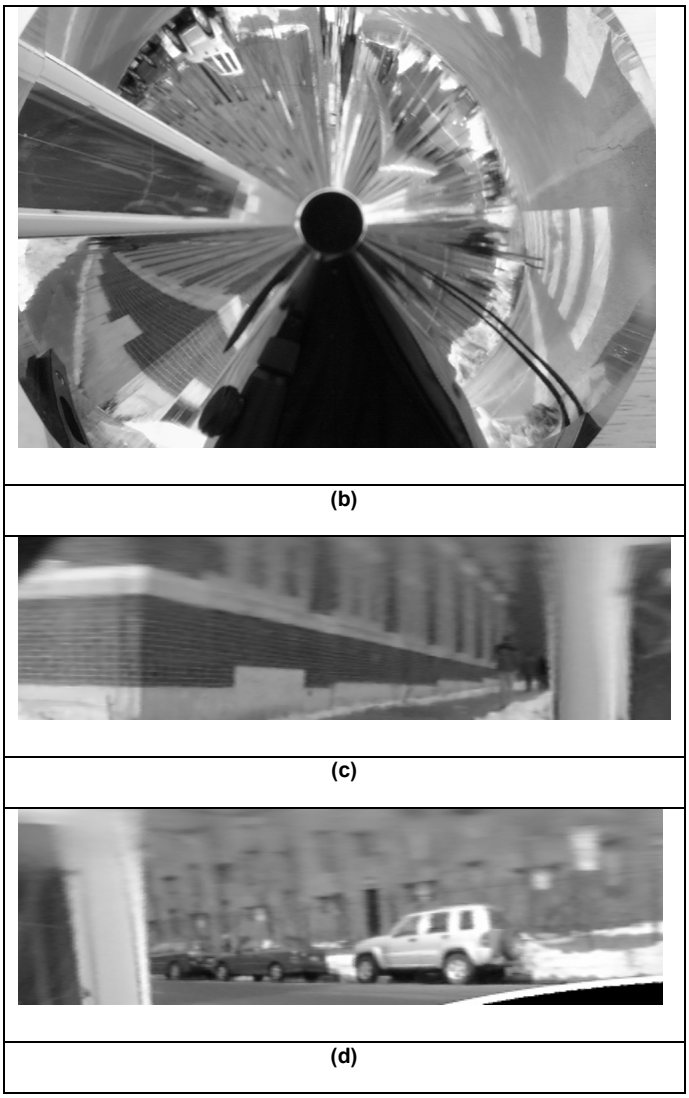

(b)

(c)

(d)

Fig. 18 (a) Best focus, f=6.5mm, F/2, 1/800 sec. (b) Best focus, f=6.5mm, F/10, 1/30 sec. (c) Unwarped from the omni-view (b), (azimuth –160 degree, elevation –6 degree), same camera parameters as the original. (d) another unwarped view from (b), (azimuth –160 degree, elevation –6 degree).

Conclusion

We have established the theory for a practical SVP cone mirror based catadioptric omnidirectional sensor. We showed why we can see images when in an SVP cone omni-cam. We showed the potential advantages and disadvantages an SVP cone mirror based system has compared to other existing SVP systems. We showed how to compute the performance parameters and how to unwrap perspectively correct image from the raw pictures taken by an

SVP cone mirror. We derived hyper-SVP formula for robustness evaluations of effects of deviations from the SVP for cone mirrors. We presented detailed quantitative analysis of the most practical image quality criteria in computer vision, i.e. the ability to resolve high frequency fine features of the scene. We showed methods and to what extent one can minimize the impact of the aberration under SVP. Our physics based simulation and real images taken confirm our theory and derivations. Both potential users and system designers can use our theory and analysis results to make the best use of a workable SVP cone mirror based omnidirectional sensor, or to avoid it when not suitable for their particular applications.

The SVP cone mirror based omni-cam provides the highest meridional image details for any omni-cam that uses only one single fixed planar imager. Although, like all other single fixed camera omni-cams, its image quality cannot compete with multi-camera or rotating camera omni-cams, the single camera SVP cone has none of their drawbacks. The rotating camera systems cannot capture all omni-view in real time, while the multi-camera systems require more resources to operate (size, power, data rate, costs,...etc.). We see potential usages of SVP cone omni-cams at least in low cost disposable military or scientific unmanned autonomous vehicles or consumer products.

REFERENCES

1. S. Baker and S. K. Nayar, "A Theory of Single-Viewpoint Catadioptric Image Formation," International Journal of Computer Vision **35,** 175-196 (1999).
2. K. Yamazawa, Y. Yagi, and M. Yachida, "Omnidirectional Imaging with Hyperboloidal Projection," in *Proceedings of the 1993 IEEE/RSJ International Conference on Intelligent Robots and Systems*, Yokohama, Japan, 1993), pp. 1029-1034.
3. T. Svoboda, T. Pajdla, and V. Hlavác, "Epipolar geometry for panoramic cameras," in *Proceedings of the 5th European Conference on Computer Vision*, 1998), pp. 218-232.

4. S.-S. Lin and R. Bajcsy, "True single view point cone mirror omni-direcitional catadioptric system," in *Proc. 8th ICCV*, Vancouver, B.C., Canada, 2001), pp. 102-107.

5. C. Geyer and K. Daniilidis, "Paracatadioptric camera calibration," IEEE Transactions on Pattern Analysis and Machine Intelligence **24,** 687-695 (2002).

6. S.-S. Lin. "OMNI-DIRECTIONAL 3D STEREO COMPUTER VISION SENSOR USING REFLECTIVE CONE MIRROR," . 2003. Computer and Information Science Department, University of Pennsylvania.

7. Y. Yagi, S. Kawato, and S. Tsuji, "Real-Time Omnidirectional Image Sensor (COPIS) for Vision-Guided Navigation," IEEE Transactions on Robotics and Automation **10,** 11-22 (1994).

8. S. Bogner, "Introduction to panoramic imaging," in *Proc. SMC Conf. 1995*, (IEEE, 1995), pp. 3100-3106.

9. D. Southwell, B. Vandegriend, and A. Basu, "A Conical Mirror Pipeline Inspection System," in *Proceedings of the 1996 IEEE International Conference on Robotics and Automation*, Minneapolis, Minnesota, USA, 1996), pp. 3253-3258.

10. J. S. Chahl and M. V. Srinvasan, "Reflective surfaces for panoramic imaging," Applied Optics **36,** 8275-8285 (1997).

11. Y. Yagi, "Omnidirectional sensing and its applications," IEICE Transactions on Information and Systems **E82D,** 568-579 (1999).

12. V. S. Nalwa. "Panoramic viewing system with offset virtual optical centers," Lucent Technologies Inc. 431401[6219090]. 4-17-2001. NJ, USA. 11-1-1999.

13. H. Hua and N. Ahuja, "A high-resolution panoramic camera," in *Proc. of the Int. Conf. on Computer Vision and Pattern Recognition*, (IEEE Computer Society, Kauai, Hawaii, 2001), pp. I-960-I-967.

14. R. Swaminathan, M. D. Grossberg, and S. K. Nayar, "A perspective on distortions," in *Proc. Int. Conf. on Computer Vision and Pattern Recognition 2003*, (IEEE, 2003), pp. 594-601.

15. D. W. Rees. "Panoramic Television Viewing System," [3505465], 1-7. 4-7-1970. USA, 2884833;2950340;3205303;3229576. 4-21-1967.

16. R. A. Hicks and R. K. Perline, "Geometric Distributions for Catadioptric Sensor Design," in *Proc. of CVPR*, Kauai, Hawaii, USA, 2001), pp. 584-589.

17. R. A. Hicks and R. Bajcsy, "Reflective surfaces as computational sensors," Image and Vision Computing **19,** 773-777 (2001).

18. A. Krishna and N. Ahuja, "Panoramic image acquisition," in *International Conference on Computer Vision and Pattern Recognition*, San Francisco, CA, 1996), pp. 379-384.

19. H. Nagahara, Y. Yagi, and M. Yachida, "Resolution Improving Method for a 3D Environment Modeling Using Omnidirectinal Image Sensor," in *ICRA 2002*, (IEEE, Washington D.C., 2002), pp. 900-907.

20. H. Ishiguro, M. Yamamoto, and S. Tsuji, "Omnidirectional stereo," IEEE Transactions on Pattern Analysis and Machine Intelligence **14,** 257-262 (1992).

21. D. W. Murray, "Recovering range using virtual multicamera stereo," Computer Vision and Image Understanding **61,** 285-291 (1995).

22. S. B. Kang and R. Szeliski, "3-d scene data recovery using omnidirectional multibaseline stereo," International Journal of Computer Vision **25,** (1997).

23. R. Benosman and J. Devars, "Panoramic stereovision sensor," in *Proc. ICPR 1998*, (IEEE, 1998), pp. 767-769.

24. S. Peleg, M. Ben-Ezra, and Y. Pritch, "Omnistereo: Panoramic Stereo Imaging," IEEE Transactions on Pattern Analysis and Machine Intelligence **23,** 279-290 (2001).

25. D. Southwell, A. Basu, M. Fiala, and J. Reyda, "Panoramic stereo," in *Proceedings of the International Conference on Pattern Recognition*, (IEEE Computer Society Press, 1996), pp. 378-382.

26. S.-S. Lin and R. Bajcsy, "High resolution catadioptric omni-directional stereo sensor for robot vision," in *IEEE International Conference on Robotics and Automation*, (IEEE RAS Robotics and Automation Society, Taipei, Taiwan, 2003), pp. 1694-1699.

27. H. Ishiguro, "Development of Low-Cost Compact Omnidirectional Vision Sensors" in *Panoramic Vision: sensors, theory, and applications*, R. Benosman and S. B. Kang, eds. (Springer-Verlag, New York, 2001), pp. 21-38.

28. M. Born and E. Wolf, *Principles of Optics:Electromagnetic Theory of Propagation, Interference and Diffraction of Light, 6 ed.* (Permagon Press, Oxford, 1984).

29. W. J. Smith, *Modern Optical Engineering: The Design of Optical Systems, 3 ed.* (McGraw-Hill, New York, 2000).

30. C. Carathéodory, Sitzungsberichte der Beyer. Akad. Wiss. Math-naturw. Abt. 1 (1926).

31. *ZEMAX Optical Design Program User's Guide Version 10.0*(Focus Software, Incorporated, Tucson, Arizona, USA, 2002).